# MICROSTRUCTURAL AND ELECTROCHEMICAL CHARACTERIZATION OF Ti-6Al-4V ELI ALLOY

A THESIS SUBMITTED TO
THE GRADUATE SCHOOL OF NATURAL AND APPLIED SCIENCES
OF
MIDDLE EAST TECHNICAL UNIVERSITY

BY

MELİH TOPÇUOĞLU

IN PARTIAL FULFILLMENT OF THE REQUIREMENTS
FOR
THE DEGREE OF MASTER OF SCIENCE

IN

METALLURGICAL & MATERIALS ENGINEERING

MAY 2006

Approval of the Graduate School of Natural and Applied Sciences.

_____

Prof. Dr. Canan Özgen
Director

I certify that this thesis satisfies all the requirements as a thesis for the degree of Master of Science.

_____

Prof. Dr. Tayfur Öztürk
Head of Department

This is to certify that we have read this thesis and that in our opinion it is fully adequate, in scope and quality, as a thesis for the degree of Master of Science.

| | |
|---|---|
| _____ | _____ |
| Prof. Dr. Şakir Bor | Assoc. Prof. Dr. M. Kadri Aydınol |
| Co-Supervisor | Supervisor |

Examining Committee Members

| | |
|---|---|
| Prof. Dr. Tayfur Öztürk | (METU, METE) _____ |
| Assoc. Prof. Dr. M. Kadri Aydınol | (METU, METE) _____ |
| Prof. Dr. Şakir Bor | (METU, METE) _____ |
| Prof. Dr. Semra Bilgiç | (Ankara Unv, CHEM) _____ |
| Assist. Prof. Dr. Caner Durucan | (METU, METE) _____ |

I hereby declare that all information in this document has been obtained and presented in accordance with academic rules and ethical conduct. I also declare that, as required by these rules and conduct, I have fully cited and referenced all material and results that are not original to this work.

Name, Last name : Melih Topçuoğlu

Signature :

# ABSTRACT


**MICROSTRUCTURAL AND ELECTROCHEMICAL CHARACTERIZATION OF Ti-6Al-4V ELI ALLOY**

Topçuoğlu, Melih
M.S., Department of Metallurgical & Materials Engineering
Supervisor: Ass. Prof. Dr. M. Kadri Aydınol
Co-Supervisor: Prof. Dr. Şakir Bor

May 2006, 93 Pages

In this study, the evolution of structure and the relationship between microstructure and corrosion behavior of the Ti-6Al-4V ELI (Extra Low Interstitial) alloy was investigated in Ringer's solution at 37 ± 0.1 $^{o}$C. Initially, different heat treatments were performed in order to obtain several microstructures which were; Widmanstätten α for furnace cooling (FC), basket-weave α for air cooling (AC), martensite (α') for water quenching (WQ) from 1060 $^{o}$C, and aged martensite for ten hours at 500, 600, 700, 800, 900 $^{o}$C. The microstructural characterizations were done by using SEM and X-ray Diffraction technique. Finally, the corrosion tests were accomplished in Ringer's solution and NaF added Ringer's solution by using open circuit potential and anodic polarization techniques, respectively.

The results showed that vanadium element removal from martensite phase and unit cell volume increase were detected during aging due to the replacement of vanadium with titanium atoms. According to the alloying element distribution

throughout the microstructure, the passive film formation due to equilibrium corrosion conditions was better in FC specimen than AC and WQ specimens. But during anodic polarization, the stability of the film in high $Cl^-$ ion concentration medium was more resistant to dissolution for WQ and aged specimens. As a result, the alloying element distribution underneath the passive film seemed to have an important role on the film formation and its stability. However, in non-equilibrium conditions, the passive film formation tendency due to the addition of NaF at 0.2M decreased because of the detrimental effects of $F^-$ ions.

**Keywords:** Ti-6Al-4V ELI, microstructure, transformation, electrochemical behavior, Ringer's solution.

# ÖZ

## Ti-6Al-4V ELI ALAŞIMININ İÇ YAPI VE ELEKTORKİMYASAL KARAKTERİZASYONU

Topçuoğlu, Melih
Y. Lisans, Metalurji ve Malzeme Mühendisliği
Tez Yöneticisi: Doç. Dr. M. Kadri Aydınol
Yrd. Tez Yöneticisi: Prof. Dr. Şakir Bor

Mayıs 2006, 93 sayfa

Bu çalışmada, Ti-6Al-4V ELI alaşımındaki iç yapı gelişimleri ve iç yapıyla korozyon davranışı arasındaki ilişki 37 ± 0.1 $^{o}$C sıcaklıktaki Ringer çözeltisinde incelenmiştir. Öncelikle, farklı ısıl işlemler gerçekleştirilerek değişik iç yapılar elde edilmiştir. Bunlar, 1060$^{o}$C'den fırında soğutma (FS) için Widmanstätten α, havada soğutma (HS) için örgü biçimli α, su verilmiş (SV) için martensit ve 10 saat 500, 600, 700, 800, 900 $^{o}$C'lerde yaşlandırılmış martensittir. İç yapı karakterizasyonu SEM ve X-Ray Difraktometre teknikleri kullanılarak yapılmıştır. Son olarak da, sırasıyla açık devre potansiyeli ve anodik polarizasyon yöntemleri kullanılarak Ringer ve NaF eklenmiş Ringer çözeltisinde korozyon testleri tamamlanmıştır.

Sonuçlar göstermiştir ki, yaşlandırma işlemi sırasında martensit fazından vanadyum elementinin çıkışı ve vanadyumun titanyum atomları ile yer değiştirmesiyle de birim hücre hacmindeki artış bulunmuştur. İç yapı genelinde, alaşım elementi dağılımı göz önünde bulundurulduğunda, denge korozyon koşullarında, pasif film oluşumu FS numunesinde HS ve SV numunelerinden

daha iyidir. Ama anodik polarizasyon sırasında, yaşlandırılmış numunelerde filmin çözünmeye karşı gösterdiği kararlılık yüksek $Cl^-$ iyonu içeren ortamlarda daha fazladır. Görülmektedir ki, pasif film altında yer alan alaşım elementi dağılımının pasif film oluşumu ve kararlılığı üzerinde etkisi olabilmektedir. Bununla birlikte, çözeltiye 0.2M NaF eklenmesiyle ortaya çıkan $F^-$ iyonlarının zararlı etkilerinden dolayı, denge dışı koşullarda pasif film oluşturma eğilimindeki düşüş göze çarpmaktadır.

**Anahtar Kelimeler:** Ti-6Al-4V ELI, iç yapı, dönüşüm, elektrokimyasal davranış, Ringer çözeltisi.

*To My Angel*

*and*

*My Family*

# ACKNOWLEDGEMENTS

The author wishes to express his deepest gratitude to his supervisor Assoc. Prof. Dr. M. Kadri Aydınol and co-supervisor Prof. Dr. Şakir Bor for their guidance, advice, criticism, encouragement and insight throughout the research.

The author also wants to express sincere thanks to Fatih Gürçağ Şen and Cengiz Tan for their kind interest during SEM studies, and Necmi Avcı for performing XRD measurements.

Thanks are to all of my friends at the Department of Metallurgical and Materials Engineering, METU, especially Barış Okatan, Alper Kınacı, Evren Tan, Güher Kotan, Tufan Güngören, Gülgün H. Aydoğdu and Ziya Esen for their support in the completion of the thesis.

Thanks are also to Hipokrat Medical Materials Production and Marketing Company for their help about material provision.

Finally, a very special thanks to my parents for their support, encouragement and trust in me throughout my life.

# TABLE OF CONTENTS

PLAGIARISM ..... iii
ABSTRACT ..... iv
ÖZ ..... vi
ACKNOWLEDGEMENTS ..... ix
TABLE OF CONTENTS ..... x
LIST OF TABLES ..... xii
LIST OF FIGURES ..... xiii
CHAPTER ..... 1
1. INTRODUCTION ..... 1
2. METALLURGY OF TITANIUM ..... 3
2.1 Background ..... 3
2.2 The Classification of Titanium Alloys ..... 4
2.2.1 Crystal Structure ..... 4
2.2.2 The Alloying Behavior of Titanium ..... 5
2.2.3 Titanium Groupings ..... 8
2.2.3.1 Unalloyed Titanium ..... 9
2.2.3.2 Alpha and Near – Alpha Alloys ..... 9
2.2.3.3 α + β Alloys ..... 11
2.2.3.4 Metastable β Alloys ..... 12
2.3 Phase Transformations ..... 13
2.3.1 Martensitic Transformations ..... 14
2.3.2 Nucleation and Diffusional Growth ..... 15
2.3.3 Thermomechanical Treatment ..... 16
2.3.4 Microstructural Developments in Titanium Alloys ..... 19
2.3.4.1 Ti-6Al-4V ..... 20
2.4 Oxidation and Corrosion ..... 31

3. BASICS OF CORROSION ..... 39
3.1 Introduction to Corrosion ..... 39
3.2 Electrochemical Kinetics of Corrosion ..... 41
3.2.1 Faraday's Law ..... 41
3.2.2 Electrochemical Polarization ..... 42
3.2.2.1 Activation Polarization ..... 42
3.2.2.2 Polarization Resistance, $R_p$ ..... 46
3.3 Passivation ..... 48
4. EXPERIMENTAL DETAILS ..... 49
4.1 Material and Specimen Preparation ..... 49
4.2 Experimental Procedure ..... 52
4.2.1 Open Circuit Potential (OCP) Measurement ..... 52
4.2.2 Anodic Polarization Measurement ..... 52
5. RESULTS AND DISCUSSION ..... 55
5.1 Microstructural Examinations ..... 55
5.2 X – Ray Diffraction Analysis ..... 61
5.3 Hardness Measurements ..... 69
5.4 Corrosion Measurements ..... 70
5.4.1 Open Circuit Potential (OCP) Measurements ..... 70
5.4.2 Activation Polarization ..... 71
6. CONCLUSION ..... 83
REFERENCES ..... 86

# LIST OF TABLES

**Table 4.1** The chemical composition of Ti-6Al-4V ELI alloy [54]. ..... 49
**Table 4.2** Heat treatments of Ti-6Al-4V ELI. ..... 50
**Table 4.3** The chemical composition of the Ringer's Solution. ..... 52
**Table 5.1** The peak indices and diffraction angles of pure α and pure β titanium for Cu – $K_\alpha$. The lattice parameters of pure α - Titanium are 2.9503 Å for "a" and 4.681 Å for "c" values and "c/a ratio" is 1.5866. For pure β - Titanium, "a" value is 3.3112 Å [56]. ..... 62
**Table 5.2** The diffraction angles and the indices of the peaks for all heat treated specimens ..... 66
**Table 5.3** Lattice parameters for the hexagonal α or α' phases and unit cell volume for all heat treated specimens and pure α-Ti. (*) was for experimental value of "a" and "c" for FC and WQ in Malinov et. al. study [9]. ..... 67
**Table 5.4** The computational results of $E_{corr}$, $I_{corr}$, $R_p$, $B$, and corrosion rate, $r$, for all specimens with respect to all surface and corrosion medium conditions... 76
**Table 5.5** The passivation potentials, $E_{pas}$ and passivation current densities, $I_{pas}$, of all heat treated specimens. ..... 77

# LIST OF FIGURES

**Figure 2.1** Influence of alloying elements on phase diagrams of Titanium alloys [1]. ..... 6
**Figure 2.2** Three-dimensional phase diagram to classify titanium alloys [1]. ..... 8
**Figure 2.3** Thermomechanical treatment of titanium alloy [1]. ..... 18
**Figure 2.4** Schematic ternary phase diagram of Ti-6Al [1]..... 19
**Figure 2.5** Processing route for fully lamellar microstructure [10]..... 24
**Figure 2.6** – Processing route for bi-modal (duplex) microstructures [10]..... 28
**Figure 3.1** Activation energy model for activation overpotential. Equilibrium state ( ——— ); polarized state ( - - - - - - - - ) [2]. ..... 43
**Figure 5.1** SEM image of Ti-6Al-4V ELI alloy after heat treatments; **(a)** Furnace Cooled (FC), **(b)** Air Cooled (AC), **(c)** Water Quenched (WQ), WQ + Aged at **(d)** 500 $^{o}$C, **(e)** 600 $^{o}$C, **(f)** 700 $^{o}$C, **(g)** 800 $^{o}$C, **(h)** 900 $^{o}$C. ..... 57
**Figure 5.2** The X – Ray diffraction pattern of pure $\alpha$ and pure $\beta$ titanium..... 61
**Figure 5.3** The X-Ray Diffraction Patterns of all heat treated specimens; **(a)** Furnace Cooled (FC), **(b)** Air Cooled (AC), **(c)** Water Quenched (WQ), WQ + Aged at **(d)** 500 $^{o}$C for 10 hrs. ..... 63
**Figure 5.3** (Continued) – The X-Ray Diffraction Patterns of aged specimens at (e) 600 $^{o}$C, (f) 700 $^{o}$C, (g) 800 $^{o}$C, (h) 900 $^{o}$C for 10 hrs. ..... 64
**Figure 5.4** The lattice parameters; **(a)** c, **(b)** a , **(c)** c/a ratio, and **(d)** unit cell volume for all heat treated specimen..... 68
**Figure 5.5** Hardness values of all heat treated specimens. ..... 69
**Figure 5.7** $E$ vs $I$ graph for **(a)** FC, AC and WQ specimens and **(b)** WQ, WQ + Aged at 500, 600, 700, 800, 900 $^{o}$C for 10 hrs specimens which had passive films on their surfaces in Ringer's solution. ..... 72

**Figure 5.8** *E* vs *I* graph for **(a)** FC, AC and WQ specimens and **(b)** WQ, WQ + Aged at 500, 600, 700, 800, 900 $^{o}$C for 10 hrs specimens for as polished surface condition in Ringer's solution. ..... 73
**Figure 5.9** *E* vs *I* graph for **(a)** FC, AC and WQ specimens and **(b)** WQ, WQ + Aged at 500, 600, 700, 800, 900 $^{o}$C for 10 hrs specimens for as polished surface condition in 0,1M NaF added Ringer's solution. ..... 74
**Figure 5.10** *E* vs *I* graph for **(a)** FC, AC and WQ specimens and **(b)** WQ, WQ + Aged at 500, 600, 700, 800, 900 $^{o}$C for 10 hrs specimens for as polished surface condition in 0,2M NaF added Ringer's solution. ..... 75

# CHAPTER 1

## INTRODUCTION

Titanium and titanium alloys are currently finding increasingly widespread use in many industries, such as aerospace applications, military and civil applications, and medical engineering, due to their desirable combination of very good mechanical properties; low densities, which give very attractive strength-to-weight ratios, very low to high temperature capability, good toughness, high stiffness allied to excellent corrosion and erosion resistance [1]. For these demanding applications functionality and reliability of components are of great importance. Therefore research aiming towards better knowledge and understanding of all processes in the manufacture of titanium components from mineral ore to finished parts are of great significance. This is not only for the purpose of developing new stronger materials but also for the optimization of already existing processes. The most commonly used titanium alloy is the two phase ($\alpha + \beta$) alloy, Ti-6Al-4V. Due to the $\alpha/\beta$ transformation in the alloy, a variety of microstructures and property combinations can be achieved through thermo mechanical processing, which permits the adaptation of properties to specific applications [1].

Titanium and its alloys are forming a continuous, stable, protective, and adherent oxide on the surface in the presence of oxygen and moisture [2]. The formation of the passive film on the surface of the titanium and titanium alloys depends on mostly the surface condition, the environment, the alloying elements in the material and the microstructure throughout the material [3]. Due to the outstanding biocompatibility of these materials, the wide variety of use in several

industries and the good combination of mechanical properties, Ti-6Al-4V ELI (Extra Low Interstitial) alloy was chosen as a material for this thesis study

The aim of this study was the electrochemical characterization of Ti-6Al-4V ELI alloy according to the microstructural evolutions in the material. The determination of the effect of obtained microstructural features on the corrosion resistance in equilibrium and non-equilibrium conditions, and the formation of film characteristics were the main focus of this thesis study.

# CHAPTER 2

## METALLURGY OF TITANIUM

### 2.1 Background

Titanium, the ninth most plentiful element and the fourth abundant structural metal making up 0.6% of the earth's crust, was first identified as a new metallic element in the mineral manaccanite by William Gregor in England in 1791, and name of Titanium was given in 1795 by the Berlin chemist Klapproth in Germany after the Titans of Greek mythology [4]. As the stable dioxide, titanium occurs in nature in different crystal modifications corresponding to the minerals rutile (93-96% $TiO_2$) [5]; (brookite, anatase) from the beach sands in Australia, India, and Mexico, ilmenite ($FeTiO_3$; 44-70% $TiO_2$) [5] and leucoxene which is an alternation product of ilmenite; mainly found in Russia [1]. Rutile, brookite and anatase all have the same chemistry, $TiO_2$, but they have different structures. After 750 $^oC$ brookite and 915 $^oC$ anatase revert to the rutile form. On the other hand, leucoxene concentrates contain up to 90% titanium dioxide [5].

The strong tendency of titanium metal to react with oxygen and nitrogen makes the production of high-purity titanium difficult. This is the main reason behind the late use of titanium as a metal. Therefore, in the middle of the $20^{th}$ century, W.J. Kroll developed a commercially attractive process, which involves the reduction of titanium tetrachloride with magnesium in an inert-gas atmosphere. As a product, porous, spongy appeared titanium formed that is called "titanium sponge". Even today it is produced only in a batch process, and no continuous process exists as for other structural metals. Because the relatively low density of this metal, 4.51 $g/cm^3$, (between those of aluminum and iron) in

combination with a high yield strength (especially in the 200-450 $^{o}$C range), good oxidation resistance at temperatures lower than 600 $^{o}$C, excellent corrosion resistance, high specific strength, excellent bio-compatibility, and its decorative appearance, the commercial interest in titanium and its alloys was prompted which explain their preferential use in the aerospace sector, the chemical industry, medical engineering. Thus, titanium is classified as a nonferrous and light metal [1, 4].

In addition, titanium can be forged, it is castable preferably investment casting method, may be processed by means of powder metal technology, it is joinable and formable and readily machinable [5].

## 2.2 The Classification of Titanium Alloys

### 2.2.1 Crystal Structure

Titanium atom has an unfilled 3d shell transition metal and can crystallize in various crystal structures. However, each modification is stable within particular temperature ranges. The complete transformation from one into another crystal structure is called allotropic transformation, and it takes place at transus temperature. This transformation temperature is called β-transus and is defined as the lowest equilibrium temperature at which material is 100% β. The β-transus temperature for pure titanium is 882 ± 2 $^{o}$C. Pure titanium, as well as the majority of titanium alloys, crystallizes at low temperatures in a modified ideally hexagonal close packed (HCP), called “alpha” (α) titanium. This structure transforms to a body-centered cubic (BCC) crystal structure, called “beta” β titanium. The density of the bcc β phase is slightly greater than that of the closer-packed hcp α phase [1].

The lattice parameters of the hexagonal close packed crystal structure in α titanium are a = 0.295 nm and c = 0.468 nm, giving a “c/a ratio” of 1.587 where

this is 1.633 for an ideally closed packed hexagonal lattice. The lattice parameter of bcc β titanium at 900 $^{o}$C is a = 0.331 nm. Because of the interstitially dissolved atoms in the hcp lattice, e.g. C, N, or O, or the substitutional atoms with smaller atomic radii than titanium, e.g. Al, the c / a ratio of the α titanium slightly increases. Polycrystalline hexagonal α titanium is extremely difficult to deform. The result of additional deformation on secondary slip systems as well as possible mechanical twinning causes the limited ductility [1].

### 2.2.2 The Alloying Behavior of Titanium

The chemical composition and the microstructure are the two factors which determine the properties of titanium alloys. The alloying elements in most Ti alloys are added to control the constitution of the alloy, to alter and/or control the transformation kinetics, and to solid-solution-strengthen one or more of the microstructural constituents [6].

The alloying behavior of titanium is readily discussed in terms of the effect of different solutes on the allotropic transformation temperature of the pure metal which is given in Figure 2.1. The chemical composition of the titanium alloys determines the properties and volume fraction of the phases, α and β. The alloying elements of titanium are classified as neutral, α-stabilizers, or β-stabilizers depending on their influence on the β-transus temperature. The β-stabilizing elements shift the β phase field to lower temperatures, while the α-stabilizing elements extend the α phase field to higher temperatures. Neutral elements have only minor influence on the β-transus temperature. The alloying elements can also be divided into substitutional solutes that their concentrations constitute the basis for commercial alloy designations and interstitial solutes. For mechanical properties point of view, α is less ductile compared with the bcc β, due to the limited deformation capability of hcp structures. The diffusion coefficient of α is more than two orders of magnitude lower than that of β.

Therefore, the resistance to creep and oxidation increases with increasing aluminum content, while simultaneously the ductility and the deformation capability deteriorate [1, 6].

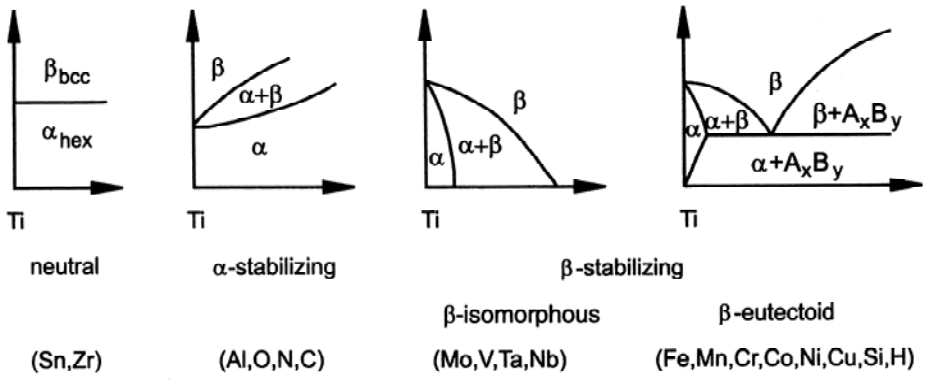



**Figure 2.1** Influence of alloying elements on phase diagrams of Titanium alloys [1].

Among the α-stabilizers, aluminum is by far the most important alloying element of titanium and also the interstitial elements oxygen, nitrogen, and carbon belong to this category. Oxygen is always present in Ti alloys and modern commercial practice permits good control of the O concentration and thus controlled levels of O are now commonly used as a strengthening addition. N and C are both soluble enough to be important as solid-solution strengtheners and to have significant effects on the nucleation of the α phase. Among these common interstitials, B is also found as an impurity in some types of alloy. Other elements such as Mg and Be may dissolve as interstitials, but their solubility is so limited that they are of little importance as solid solution elements. In addition to extending the α phase field to higher temperatures, the α-stabilizers develop a two-phase α + β field. β-stabilizing elements are subdivided into β-isomorphous and β-eutectic elements. Of these, the β-isomorphous elements, e.g. Mo, V, Nb and Ta, are by far more important due to their much higher solubility in titanium. On the other hand, even very low volume fractions of β-eutectic elements, e.g. Fe, Mn, Cr, Co, Ni, Cu, Si, and H, can lead to the formation of intermetallic

compounds and they decrease the transformation temperature. Si atoms tend to segregate to dislocations and thus effectively prevent dislocation climb, which improves creep behavior. The solubility of H is very high in the β phase and relatively low in the α phase, because the Ti-H system forms a eutectoid and the solubility of H in the α phase in equilibrium with titanium hydride is small. In addition to the transition metals, the noble metals Au, Cu and Ag as well as the heavy transition metals Pt and Pd are eutectoid formers. Sn, Hf and Zr are considered neutral elements since they have (nearly) no influence on the α/β phase boundary. As far as strength is concerned, they are not neutral since they primarily strengthen the α phase. Zr tends to homogenize fine silicide precipitates [1, 4-6]

Usually titanium alloys are classified as α, α+β, and β alloys, with further subdivision into the near-α and metastable β alloys [1]. According to the three–dimensional phase diagram given in Figure 2.2, the α alloys comprise commercially pure (CP) titanium and alloys exclusively alloyed with α-stabilizing elements and/or neutral elements. If minor fractions of β-stabilizing elements are added, they are referred to as near-α alloys. The α + β alloys, the most widely used alloy group, having a β volume fraction ranging from about 5 to 40% at room temperature. If the proportion of β-stabilizing elements is further increased to a level where β no longer transforms to martensite upon fast quenching, the alloys are still in the two-phase field and the class of metastable β alloys is reached. In metastable β alloys the β phase can be effectively strengthened by fine omega precipitates. Unfortunately, these high strength levels are usually accompanied by falls in ductility. These alloys can still reveal an equilibrium α volume fraction of more than 50%. Finally, the single-phase β alloys mark the end of the alloying scale of the conventional titanium alloys [1].

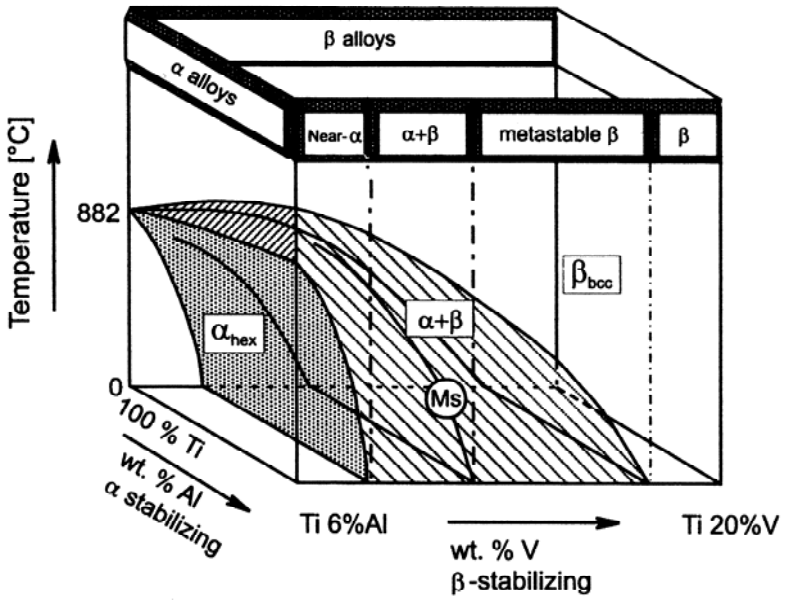



**Figure 2.2** Three-dimensional phase diagram to classify titanium alloys [1].

### 2.2.3 Titanium Groupings

Today more than 100 titanium alloys are known, of which, however, only 20 to 30 have reached commercial status. Of these, the classic alloy Ti-6Al-4V covers more than 50% of usage. Another 20 to 30% are unalloyed titanium [1]. When considering unalloyed and alloyed titanium, it is common to group the materials as;

- Unalloyed Titanium
- Alpha and Near-alpha Alloys
- Alpha-beta Alloys
- Metastable beta Alloys

#### 2.2.3.1 Unalloyed Titanium

There are several grades of unalloyed titanium. The primary difference between grades is oxygen content. Grades of higher purity (lower interstitial content) are lower in strength, hardness and transformation temperature than those higher in interstitial content. Unalloyed titanium is selected for its excellent corrosion resistance, especially in applications where high strength is not required [7]. However, for adjusting the α grain size to a desired level, thermomechanical treatment is performed in the α phase field at 200-300 $^{o}$C or even at room temperature [4]. The four important commercially pure titanium Grades, 1 to 4 cover a room temperature ($T_R$) tensile strength level of 240 to 740 MPa with a decrease in formability due to the decrease in the ease of twinning. Of these, Grade 1 has the lowest strength level, excellent cold formability and corrosion resistance. It is used for deep drawing applications and as cladding alloy for steel reactors. Grade 2, with tensile strength levels between 390 and 540 MPa, is the most popular cp titanium grade. Grade 3 is used for pressure vessel applications where higher strength and weight is a concern. Grade 4 has the highest strength of up to 740 MPa and is preferentially used for mountings and fittings [1, 4].

#### 2.2.3.2 Alpha and Near – Alpha Alloys

Alpha alloys are primarily used in the chemical and process engineering industry. Excellent corrosion behavior and deformability are of prime concern while high (specific) strength only ranks second. As an interstitial alloying element, the oxygen content differs the various commercially pure (cp) titanium grades and increases strength with a simultaneous reduction in ductility. Elements like carbon and iron are impurities brought into the alloy via the manufacturing process, only oxygen is intentionally alloyed to reach the required strength levels of cp titanium grades [1]. The high solubility of the interstitial element oxygen and nitrogen makes titanium unique among metals and also creates problems not of concern in most other metals. For example, heating titanium in air at high

temperature results with inward diffusion of oxygen (and nitrogen), not only in oxidation but also in solid-solution hardening of the surface. A surface-hardened zone of “alpha-case” (or air-contamination layer) is formed. Normally, this layer is removed by machining, chemical milling, or other mechanical means prior to placing a part in service because the presence of alpha-case reduces fatigue strength and ductility [7].

Alpha alloys cannot be strengthened by heat treatment and generally, they are annealed or recrystallized to remove residual stresses induced by cold working. Alpha alloys have good weldability because they are insensitive to heat treatment and mostly have poorer forgeability and narrower forging temperature ranges than alpha-beta or beta alloys, particularly below at beta transus [5]. The Ti-8Al-1Mo-1V was the first titanium alloy for high temperatures but stress corrosion problems because of high Al contents, all conventional titanium alloys in use today are limited in aluminum content to a maximum of 6%. The follow up alloy, Ti-6Al-2Sn-4Zr-2Mo (Ti-6-2-4-2), and in the 1970s investigations exhibited that addition of Si up to 0.1% improves the creep behavior. At high temperatures Si would precipitate at high temperatures on dislocations, thus effectively hindering their climb and likewise deformation. Since then all new high temperature titanium alloys have been alloyed with up to 0.5% of Si [1].

Near-α titanium alloys, which contain Al, Sn, and/or Zr inside, are preferred for high temperature applications as well as cryogenic applications since it combines the excellent creep behavior of α alloys with the high strength of α + β alloys. Their upper operating temperature is limited to about 500 to 550 $^{o}$C [1].

If higher strength levels are required, Ti-5Al-2Sn is a good choice, especially for hydrogen tanks and pressure vessels [1]. The extra-low-interstitial alpha alloys (ELI grades) retain ductility and toughness at cyrogenic temperatures, and again Ti-5Al-2.5Sn ELI has been used extensively in such applications [7].

#### 2.2.3.3 α + β Alloys

In this system, alloys contain one or more alpha stabilizers or alpha-soluble elements and more beta stabilizers. After solution treatment, these alloys retain more β phase than do near-α alloys. The specific amount depends on the quantity of beta stabilizers present and on the heat treatment [5].

Alpha-beta alloys can be strengthened by solution treating, which is usually done at a temperature high in the two-phase field and is followed by quenching in water, oil, or other soluble quenchant, and aging to precipitate α and produce a fine mixture of α and β in the retained or transformed β phase. The specific response of beta transformation depends on alloy composition, solution-treating temperature, cooling rate and section size [5].

Solution treating and aging can increase the strength of alpha-beta alloys from 30 to 50%, or more, over the annealed or over-aged condition. Response to solution treating and aging depends on section size; alloys relatively low in β stabilizers, for example Ti-6Al-4V which is by far the most popular titanium alloy and accounting for about 45% of total titanium production [7], have poor hardenability and must be quenched rapidly to achieve significant strengthening. As the content of β stabilizers increases, hardenability increases. The strength that can be achieved by heat treatment is also a function of the volume fraction of beta phase present at the solution-treating temperature. To produce the desired mechanical properties in the final product, alloy composition, solution temperature, and aging condition must be carefully selected. So, in the early 1950s in the United States at the Illinois Institute of Technology, to answer the industrial needs, Ti-6Al-4V was developed which is especially used in the aerospace industry, and also used in reaction vessels, heat exchangers and gas compressors. Other α + β alloys like Ti-6Al-6V-2Sn and Ti-4Al-4Mo-2Sn-0.5Si (IMI 550) were primarily developed for high strength. High strength and high toughness is realized with Ti-6Al-2Sn-4Zr-6Mo (Ti-6-2-4-6) [1, 5].

#### 2.2.3.4 Metastable β Alloys

Over the last few decades the importance of metastable β alloys has steadily increased. The beta alloys of the metastable beta system are richer in β-stabilizers and leaner in alpha stabilizers than α + β alloys. Depending on the amount of β stabilizing elements, β alloys can be retained in a mestable form upon cooling to room temperature at moderate to high cooling rates which means no α precipitation is taking place during cooling [4]. Processing of β titanium alloys usually consist of a hot working operation, which is normally performed in the (α + β) phase field for the leaner beta alloys, and preferentially in the β field for the richer beta alloys, followed by a heat treatment consisting of a solution treatment followed by quenching and a subsequent aging treatment. Above the β transus temperature, a solution heat treatment causes a coarsening of the β grains and the temperatures below the transus leads to the precipitation of primary α ($\alpha_P$). The heat treatment temperature controls the volume fraction of $\alpha_P$. While the thermomechanical treatment leads to a globular $\alpha_P$ shape, without a treatment a needle-like $\alpha_P$ shape develops. These alloys have excellent forgeability and can be hardened to extremely high strength levels of more than 1400 MPa. The complex microstructure enables the designer to optimize for both high strength and high toughness [1, 8].

Proper selection of temperatures and deformation are the parameters which controls the β grain size and size distribution. During thermomechanical treatment, a film-like α precipitation occurs on the grain boundaries. By rapid cooling from the β phase field, the precipitation of this boundary α can be prevented for small sections [1]. Also, two different approaches have been given to avoid this film-like α precipitation. One is to obtain a bi-modal microstructure similar in the α + β alloys and the second one is creating a necklace type of microstructure [4].

At lower temperatures, like 400 to 600 $^{o}$C, secondary α precipitates finely distributed homogeneously or inhomogeneously, depending on being in lean beta alloys or in richer alloys, respectively. By varying the aging temperature, time and solution treatment temperature, the volume fraction and size of the secondary α can be controlled. Also in lean alloys, precipitation of coherent ω phase can be seen at low temperatures which may cause embrittlement. And higher β stabilizing element forms intermetallic compunds [1].

The advantages of beta alloys in comparison with alpha-beta alloys are their density, lower creep strength, and lower tensile ductility in the aged condition. Ti-5Al-4Mo-4Zr-2Sn-2Cr (Beta-CEZ) developed in France, Japanese alloy Ti-4.5Al-3V-2Fe-2Mo (SP 700) and Ti-10V-2Fe-3Al (TIMETAL 10-2-3) can be given as an example for metastable β alloys [1, 8].

### 2.3 Phase Transformations

Upon cooling from the β phase field of titanium the most densely packed planes of the BCC β phase {110} transform to the basal planes {0001} of the hexagonal α phase by a nucleation and shear type process. The orientation relationship of the transformation of the slip planes for the bcc β titanium into the HCP α titanium is given by a Burgers-Relationship which yields 12 variants [1]:

$$\{0001\}_{\alpha} // \{110\}_{\beta}$$
$$\langle 1120\rangle_{\alpha} // \langle 111\rangle_{\beta}$$

The metallographic microstructure reflects this orientation relationship by martensitically or by a nucleation and growth of the individual α lamellar packets within the prior β grains [1, 4].

### 2.3.1 Martensitic Transformations

Martensitic transformation results in a microscopically homogeneous transformation of the BCC into the HCP crystal lattice, with a cooperative movement of atoms. The two different crystal structures of athermal martensites: the hexagonal martensite which is designated α', and the orthorhombic martensite which is designated α", are formed by quenching of the BCC β phase of pure Ti and dilute Ti-alloys when the martensite start temperature, $M_s$, is crossed. The most prevelant type is α', which can occur in two limiting morphologies: massive or lath martensite (high purity Ti and very dilute alloys, α or near-α alloys) and "acicular" martensite in alloys with slightly higher solute contents (lower $M_s$), which occurs as an intimate mixture of individual α plates, each having a different variant of the Burgers relation. For alloys with high $M_s$ temperatures (α or near-α alloys), martensite occurs as colonies of parallel-sided platelets, the platelets in each colony in general having the same variant of the Burgers orientation relationship to the β matrix and being separated from each other by low-angle grain boundaries. The orthorhombic martensite α", which is characterized by good deformability, seems to occur mainly in Ti-alloys with β stabilizers of the transition metals Mo, Nb, Ta, W, Re and in Ti-alloys with Al + V. The lattice parameters of α" are strongly dependent on solute content, and the α" crystal structure is sometimes conveniently viewed as a distorted hexagonal structure. The change in morphology and internal substructure in the martensite is not dissimilar to that which occurs in ferrous alloys with increasing carbon or austenite stabilizing alloying element content. According to the martensitic transformation, strength is slightly increased compared to α titanium [1, 4, 8, 9].

In some of (α + β) and β titanium alloys, the occurrence of face centered orthorhombic (FCO) and FCC martensites has also been reported [8]. The FCO martensite seems to have the morphological characteristics of $\left\{10\bar{1}1\right\}_a$ twinned hexagonal martensite and the presence of interstitials results in the distortion from the hexagonal to the FCO structure by a similar mechanism to the BCC to BCT

(body-centered tetragonal) distortion which arises from interstitial carbon in martensite in steels. As a result of strain, martensite may be induced in the metastable β for alloys in which $M_s$ is below and $M_f$ above room temperature, $T_R$ [8].

On the other hand, the FCC martensite is not apparently related to the hexagonal or FCO types. It has been reported that it occurs only on quenching from a temperature range low in the β field in (α + β) alloys and it may be a "thin foil" artifact arising from a relaxation of stresses in the metastable β in thin section or as a result of hydrogen contamination during electro-polishing. By X-ray diffraction of bulk specimens the FCC structure has not been positively identified [8].

### 2.3.2 Nucleation and Diffusional Growth

Diffusion is considerably lower in HCP α titanium than in BCC β titanium because of the densely packed atoms in HCP. The diffusion coefficient of α titanium is at least two orders of magnitude smaller than that of β titanium [4].

In Ti-alloys with intermediate solute contents, the decomposition of the β phase occurs as a nucleation of α at β grain boundaries (coarse "aligned α") and subsequent diffusion controlled growth into the retained β phase, at sufficiently low cooling rates from the single β phase field into the α + β field. The resulting microstructure, called Widmanstätten α, consists of colonies of parallel α plates having the same crystallographic orientation which belongs to a single variant of the Burgers orientation relation with regard to the parent β matrix, and those are separated by plates of the retained β phase. The higher β stabilizer added Ti-alloys, which have lower transformation temperature or increased cooling rate, the colonies become progressively smaller, exhibit fewer platelets, and appear to nucleate independently of the β grain boundaries. The characteristic microstructure, "basket-weave" structure, forms by the distribution of these

smaller colonies over all possible variants of the Burgers orientation relationship [4, 10-15].

The Widmanstätten platelets are surrounded by β-stabilizing alloying elements enriched layers of the retained β phase which occur as the result of rapid diffusion of these elements at or ahead of the migrating interface. The cooling rate and alloy content control the thickness and continuity of the retained β layers and it is metastable and may undergo a subsequent strain-induced transformation. These layers form a continuous network (~0.2 μm thick) around the α platelets in the α + β alloys, whereas in the α and near-α alloys they might be discontinuous and smaller than 0.1 μm thickness. On quenching, such layers may also occur but to a much lesser extent. In this situation the α transformation product may be more correctly described as bainite [8, 11, 15].

Solution treating the alloy in the (α + β) field gives a duplex (α + β) structure. Indication of the β-stabilizing alloying elements segregation and the phase proportions are given in the pseudo-binary equilibrium diagram. Upon cooling, the β transforms into martensite or Widmanstätten α as before or, if it is sufficiently enriched, i.e. for low solution treatment temperatures, is retained at $T_R$ [8].

### 2.3.3 Thermomechanical Treatment

The microstructure has a substantial effect on the properties of titanium alloys. The microstructure of Ti alloys can be varied and controlled or manipulated in a degree of freedom by thermomechanical treatment (TMT), which can perturb or alter the transformation mechanisms. Also, the alloy class and type controls the nature and degree of microstructure obtained [16]. For conventional titanium alloys, the size and arrangement of the two phases α and β describes the microstructure. The two extreme cases of phase arrangements are the lamellar and the equiaxed microstructures. The lamellar form is generated upon cooling from

the β phase field, while equiaxed one is a result of a recrystallization process and both structures have a fine as well as a coarse arrangement of their two phases [1, 8]. In most of the commercially important titanium alloys, the mechanism of the β phase during cooling dominates the development of titanium microstructure [16].

Thermomechanical treatments generates different microstructures as a complex sequence of solution heat treatment, deformation (by hot rolling or forging, extrusion or spinning), recrystallization, aging, and annealing for stress relief as schematically outlined in Figure 2.3. To achieve the desired microstructure, controlling the deformation rate at any particular temperature is important. The principal effect of working is to alter the morphology of the primary α phase which is formed by nucleation and growth in the early stages of working and by subsequent plastic deformation during subsequent working, leading to a recrystallization and globularization of α. For the morphology of the α, the amount of plastic work, strain rate and temperature are important. The strain rate and temperature are critical because of a dynamic competition between in situ recovery and the plastic work storage which will subsequently drive the recrystallization reaction. The occurrence of this recovery reaction means that there is not usually a unique combination of temperature and time to produce a given microstructure [16, 17]. By finish-forging high in the (α + β) phase field, the prior β grain size may also be refined [8]. On the other hand, the presence of the texture in most of the hot worked products should be mentioned. The texture to be expected due to TMT is not only very sensitive to working temperature and amount of strain, but is also very sensitive to working methods [16].

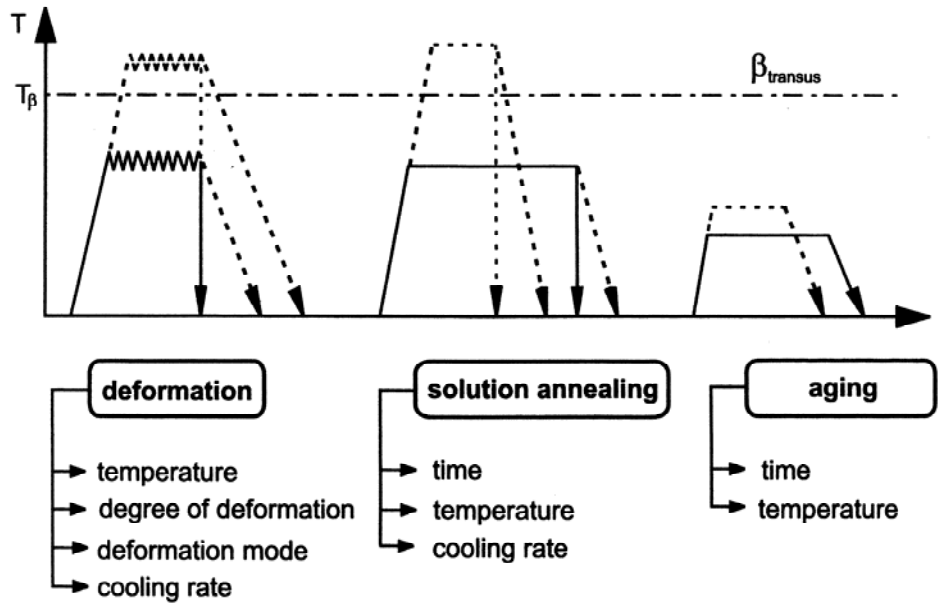



**Figure 2.3** Thermomechanical treatment of titanium alloy [1].

Ding et. al. [17] investigated the variation of microstructure under different hot working conditions by using strain rate, which caused a slight increase in the phase transformation and the degree of dynamic recrystallization, and temperature as the working parameters. According to their experimental results, the prior and the secondary α lamellar structure was the general microstructure and the grains were fibrous, when the Ti-6Al-4V was processed in the (α + β) phase field and only martensitic microstructure and elongated grains were seen, when processed in the β phase field. They grouped the lamellar morphology under five different types as the retained prior α which was the none-distorted prior α platelets, the distorted α which was distorted α platelets, segmented α which was spheroidized prior α lamella, the diffused α and the secondary α (transformed β) lamella zones. They reported that because the mechanical deformation retarded the nucleation and the growth of the new phases, the phase transformation occurred more in the "dead or unworked" zone rather than in the deformation zone in the (α + β) phase field which was also mentioned by Hammond and Nutting [8]. In addition to that, the dynamic recrystallization was seen only in the β phase field, not in the (α + β) phase field.

As a result of slower kinetics of nucleation and growth reaction because of higher amounts of β stabilizing elements, a competition develops between heterogeneous nucleation of α at prior β grain boundaries and intragranular nucleation of α. The grain boundary α, which is a general result of this competition, has a deleterious effect on properties. As previously mentioned, TMT is the acceleration of the nucleation and growth kinetics for intergranular α nucleation. Shortly, mechanical working makes the grain boundary α less continuous and less deleterious to properties by breaking up and recrystallizing it [16].

### 2.3.4 Microstructural Developments in Titanium Alloys

The β-transus temperature, $T_\beta$, which separates the single β phase field from the two phase α + β field, is a central point for thermomechanical treatment [1]. It is important to understand the competition between the nucleation and growth of α phase and the martensitic decomposition of the β phase [16]. To illustrate this point, a schematic vertical section from Ti-6Al-4V phase diagram is shown in Figure 2.4.

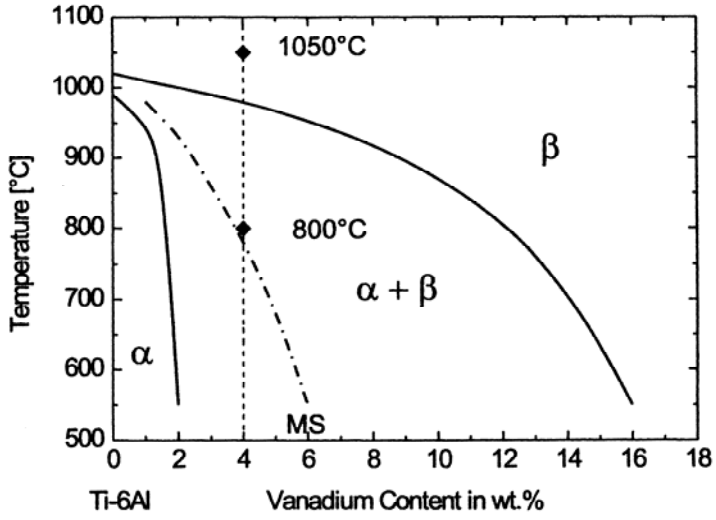



**Figure 2.4** Schematic ternary phase diagram of Ti-6Al [1].

#### 2.3.4.1 Ti-6Al-4V

One of the most widely used titanium alloy, which has the greatest commercial importance in the various industries and applications and is being responsible for more than 50% of titanium output in the world, is an alpha-beta type, with 6wt% aluminum stabilizing the α phase and 4wt% vanadium stabilizing the β phase, forming Ti-6Al-4V [5, 18, 19].

In Ti-6Al-4V, addition of aluminum partitions selectively to the α phase and forms solid solution strengthening in the alloy. The Al concentration is usually held to 6wt% or less in titanium to prevent ordered $DO_{19}$ phase, which is known as secondary α, $\alpha_2$, and results in degradation of ductility, toughness and stress corrosion cracking. The V in Ti-6Al-4V is not very soluble in the α phase and is rejected from α. Accordingly the V element is concentrated in small regions of the β phase and β phase forms uniformly throughout the predominantly α matrix [6]. This is consistent with the study of Gil et. al. [11]. They evaluated the Al and V concentrations by means of an analytical microscope and found that Al content decreases from the center of the α phase through β phase. Inversely, V content increases along the same direction because of a β-stabilizing element [11].

Because the boundary migration of these two phases requires extensive amount of diffusion, this two phase mixture is stable with respect to coarsening. As a result, Ti-6Al-4V exhibits relatively fine microstructures and addition of β-stabilizing element such as V serves solid solution strengthening in the β phase and by refining the microstructure overall alloy strengthening is established.

In order to produce refined martensitic or diffusionally controlled transformation products at subsequent cooling, the grain size should be as small as possible [20]. Ivasishin and Teliovich [20] compared steels and titanium alloys according to the grain size. They explained that titanium alloys has behaved different than steels due to the formation of fine β microstructure. Transformation to a single-phase β has developed by a movement of the α / β boundaries until the

β phase becomes the only phase present. Unless faster heating rates were applied, the immediate grain growth would occur after the dissolution of primary α phase. And also, β grain size could not be reduced by subsequent heat treatments if coarse β grain microstructure once formed. For rapid heating of the coarse-grained titanium alloys which recovers by the end of transformation no further change in grain size has taken place above the β-transus. As in the Fujii's study [12], the kinetics of grain growth depends on the particular chemistry of the high temperature phase, such that grain growth inhibiting elements content in solid solution or in the form of precipitates. Also, during studies of Stanford and Bate [21] on variant selection of Ti-6Al-4V occurred in diffusional transformation, they showed that on heating from room temperature to the β transus, the β phase in Ti-6Al-4V grew epitaxially from the pre-existing β phase, rather than to nucleate new β grains. Therefore, the texture formed during deformation would be modified by grain growth from pre-existing β orientations in the starting material during continuous heat treatment, as also seen in the Semiatin et. al. [22] work. They also reported that the peak grain size was strongly dependent on the peak temperature and heating rate. Lower heating rates and higher peak temperatures gave rise to coarser grain sizes. Ivasishin et. al. [23] did the similar work under isothermal heat treatment and, found that beta grain growth under isothermal annealing conditions was strongly affected by texture in materials and did not have a constant grain growth exponent and activation energy. They also suggested that strict control of initial texture was required in thermomechanical processing.

The microstructure of Ti-6Al-4V has various types and depends on the cooling rate from the β phase field, prior heat treatment and the chemistry [1, 11, 18]. The micro constituents and microstructures are divided into grain boundary allotriomorph α, globular or primary α (called bi-modal microstructure when the globular α is surrounded by Widmanstätten platelets), Widmanstätten, basketweave, and martensitic according to the phase transformation of β/α [18]. Also the bi-lamellar microstructure is recently described, in which the soft, single phase β lamellae, lying between the α platelets in a Widmanstätten structure, are hardened by fine α plates [10]. At room temperature, the microstructure at

equilibrium consists mainly of the α phase (HCP) with some retained β phase (BCC) [18] and β phase is stabilized as a result of vanadium enrichment [9].

When Ti-6Al-4V is slowly cooled from the β phase region, formation of α phase is seen below the β-transus temperature. The result of the decomposition of β phase by a nucleation and growth mechanism, the structure of α which is formed are the grain boundary allotriomorph α and Widmanstätten α-plates or laths which consist of the sets of parallel plates with a crystallographic relationship (α plate basal plane is parallel to a special plane $\{110\}_\beta$ in the β phase) to the β. These Widmanstätten plates often nucleate at the α-allotromorphous and grow towards the matrix with sharp and straight surface relief, which all have a lenticular shape. When the cooling rate increases, these plates become thinner and plate size increases when the cooling rate decreases. Also, the decrease in the cooling rate results the formation of α phase nucleated in the matrix ($\alpha_M$) by the ease of alloy element arrival to the nucleation sites in the β matrix. For allotriomorph α phase point of view, there is a certain decrease in size of the phase when the cooling rate increases because of a bigger diffusivity in lower cooling rates [11]. Malinov et. al. [24] measured also the formation of these grain boundary α phase and homogeneously nucleated α phase within the β grains in Ti-6Al-4V and Ti-6-2-4-2 alloys by using resistivity method. Their work showed that upon cooling from the β homogenization field down to 900 $^oC$, only the formation of grain boundary α occurred after isothermal exposure at that temperature. But when the undercooling increased further, some portions of the α phase nucleation and growth within the β grains was also observed in addition to the grain boundary α phase again after isothermal exposures. Also, Malinov et. al. [9] showed that the retained β phase after slow cooling in the furnace by using the room and high temperature synchrotron radiation HR-XRD method, and again with the help of this method they found that *hkl* reflections of α phase not having $l = 0$ were formed with different “c” and the same “a” lattice parameters due to the different precipitation temperatures of alloying elements of the α phase and the different amounts of the phases during slow continuous cooling. These results were confirmed by the diffraction patterns taken at room temperature before and after

high temperature experiments. The reflections of the α phase were shifted to lower 2θ angle implying increased lattice parameters, mostly in "c-axis", due to the increased amount of the oxygen during high temperature exposure. The X-ray diffraction analysis and microstructural observations were also studied by Jovanović et. al. [25]. They used investment cast Ti-6Al-4V alloy for experiments which were included different annealing temperature applications and cooling rates from those temperatures. They observed α phase, which formed a typical Widmanstätten structure, and weak β phase reflections in the diffraction patterns after furnace cooling and air cooling, but after water quenching only α' martensite formation was seen with an exception at 1050 $^{o}$C quenched case. They also observed that the increase in the annealing temperature caused the α plate thickness increase and lower cooling rate produced thicker α plates than air cooling from the same annealing temperature. Additionally, they concluded that with the decrease in the annealing temperature upon air cooling has caused a decrease in the volume fraction of acicular α and β phases and an increase in the primary α ($\alpha_P$), whereas that was not seen in the furnace cooling condition which was full of primary α. And these cooling conditions and obtained microstructures showed that water quenching exhibited a higher hardness values than air cooling and furnace cooling which had the lowest value.

Lütjering [14] described the microstructural constituents of fully lamellar α + β titanium alloys as large equiaxed β grains, continuous α layers at β grain boundaries, the α colony size and the size of individual α lamellae. These types of microstructures are formed according to the scheme given in Figure 2.5 below**.** After deformation either in the α + β phase field or in the β phase field, a homogenization treatment is applied in the β phase field. The final microstructure and the extent of α-layers at β grain boundaries depend on the cooling rate from the homogenization temperature. There is no alloying element partitioning effect is present in the fully lamellar microstructures, so only aging treatment or stress relieving treatment is applied after step I [10, 14].

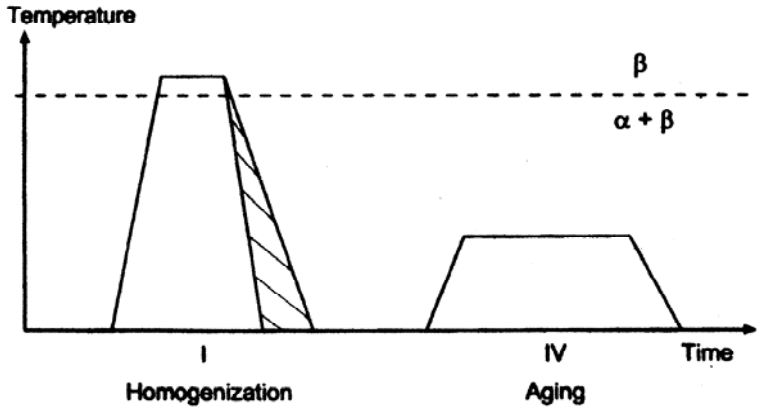



**Figure 2.5** Processing route for fully lamellar microstructure [10].

The formation of Widmanstätten structure was studied by several scientists and engineers. Fujii [12] found that the α phase first precipitated at the grain boundaries of the β matrix and by depending on the temperature drop, the growth of the side-plate α phase was observed from the grain boundary α phase into the β matrix. This side-plate α nucleation has been observed in transgranular or heterogeneous form, according to the high or low degree of undercooling, respectively. In this transformation behavior, the β stabilizing element Vanadium has an important role by concentrating near the grain boundary α phase during its formation. These results were obtained after solutionization at 1050 $^{o}$C at 20min., rapid cooling to between 800 to 850 $^{o}$C (in the α + β region), holding there for different time intervals and helium gas quenching from those temperatures.

Ahmed and Rack [13] applied β solution treatment at 1050 $^{o}$C for 30min. and ending the treatment with water or helium gas quenching by using Jominy bar which is coated with BN to minimize oxidation. They obtained different microstructures at varying cooling rates. At 525 $^{o}$C/s, they had hexagonal α' martensite but at 410 $^{o}$C/s, a second α morphology (massive α) was observed for Ti-6Al-4V which had a blocky appearance and a hexagonal crystal structure (acicular α' martensite) with a heavily dislocated internal substructure under TEM analysis. At slower cooling rates < 20 $^{o}$C/s two different types of grain boundary α obtained; type 1 having "zigzagged" appearance nucleated near or at the prior β

grain boundary and type 2 “normal” appearance seemed to have grown from the “normal” grain boundary α layer, and at the lowest cooling rate (1.5 $^{o}$C/s), the formation of the grain boundary α was seen where the intra-granular micostructure was full of classical “basketweave” Widmanstätten morphology. So they suggested that for fully martensitic microstructure, higher cooling rates than 410 $^{o}$C/s should be applied otherwise, a massive transformation might be observed.

The effect of cooling rate on the microstructure was also studied by Gil et. al. [26] and their another study in (2001) [11]. Gil and his co-workers used different temperatures, varying time intervals and cooling rates in the tubular furnace under argon atmosphere. Their results showed that the grain size increase took place when the temperature increased with time (mostly first 15 min. of the treatment) at a very fast rate to a point where grain boundary area per unit volume ratio and the interfacial energy per unit volume decreased. This means driving force for grain growth was lower. By using the solute drag theory, they explained the grain growth as a faster movement of the boundary by the diffusion of solute elements behind the boundary as a result of the phase transformation.

The grain size effect on β to α transformation indicated that the larger β grain size has produced the smaller α Widmanstätten plate width which was the result of the decrease in the starting temperature of the β to α transformation. They gave brief explanation about the transformation and formation of Widmanstätten α phase which has been the continued transformation of nucleated α phase by growth and coarsening as needles or plates within the β grains. They evaluated the Al and V content in the center of the plate and radially outwards at different distances by means of an analytical microscope and found that vanadium content has increased from the center through the β phase. And also opposite to V, Al content decreases along the same direction. These Widmanstätten plate sizes have increased due to decrease in the cooling rate because of bigger diffusivity at lower cooling rates. At low cooling rates, they found that α phase nucleation occurred in the matrix ($\alpha_M$) while the α-Widmanstätten ($\alpha_W$) has been growing by the ease of

atom movement in the matrix. So, this resulted an increase in the ratio of $\alpha_M$ / $\alpha_W$. If the cooling rate increased, the Widmanstätten colony size would decrease which was the reason of strength difference between the matrix and the coarser α-layer present at β grain boundaries causing preferential plastic deformation [11, 26]. This is consistent with Filip and his friends study. Filip et. al. [27] studied on fractographic examinations in Ti-6Al-4V and Ti-6Al-2Mo-2Cr alloy systems. Their results showed that large grain size displays intergranular fracture faces with dimensions corresponding to the grain size and for the fine grained structure the grain boundary fracture was reduced due to the increase in the cooling rate.

Opposite to the cooling treatments from the β phase, phase evolution of Ti-6Al-4V was also studied during continuous heating. Sha and Guo [28] found that at 970 $^{o}$C, firstly the transformed β phase, which contains less vanadium than equilibrium demands, transformed to high temperature β phase, and whole microstructure had transformed into β phase when the temperature reached to 1010 $^{o}$C by using differential scanning calorimetry (DSC) technique to a system which has transformed β phase and blocky α phase. The blocky α phase could not transform until the temperature high enough because of the stability of the phase gained by less β stabilizing element vanadium and more α stabilizing element aluminum content. They concluded that transition of primary α phase to β phase has started after the transition of transformed β phase to high temperature β phase has completed.

Similar to those above studies, Stanford and Bate [21] were also done phase transformation experiment using Ti-6Al-4V. But they tried to emphasize on the variant selection of the transformed structure by using Scanning Electron Microscopy (SEM) and Electron Backscatter Diffraction (EBSD). The variant selection was explained in their study as the occurrence of the individual orientation (or variants) more frequently than the other under certain conditions. To observe the selected variants and the textures exactly which were seen in the alloy system, they used furnace cooled and slow cooled samples. Their results showed that when two adjacent grains had a close (110) pole, α precipitation at

the grain boundary would occur with (0001) parallel to that particular pole in preference to the other five possible (110) poles where 6 is the number of variants within each prior β grain from the possible 12. So, they concluded that diffusional transformation exhibited strong preferred orientation. But if there was no relationship between the adjacent β grains, there could be any number of variants produced on either side of the boundary. Also there would be a third possibility which was given as the close orientation and sharing of (110) poles. In that case it was found that a number of variants could be formed on either side of the β/β boundary, and α variants shared (0001) pole. They showed that those possible variant selections had an effect of grain boundary α formation and found that grain boundary α precipitation could be profilic and did not form from one growing nucleus. They explained that because of nucleation occurred just below the β-transus, partitioning of the vanadium ahead of the transformation front was inhibited by rapid growth of the α which prevented the retention of the β layer around the grain. This result is nearly matching to the Fujii's [12] study about continuous cooling transformation of α + β alloys for grain boundary α formation point of view. Stanford and Bate [21] determined that the Widmanstätten α plates chose an orientation according to the Burgers relationship during growth was initiated from the grain boundary and the c–axis of the α was said to be adopted that same orientation.

The fully lamellar structure is turned into the bi-modal (duplex – globular or primary α) microstructure by thermomechanical treatment, which is firstly deformation of lamellar structure and then recrystallization in the α + β phase field and cooling down to room temperature as described by Lütjering studies in (1998) [10] and (1999) [14]. He figured out the formation of the microstructure by a four step process, which are homogenization in the β phase field (I), deformation in the α + β phase field (II), recrystallization in the α + β phase field (III), and aging at lower temperatures (IV), shown schematically in Figure 2.6. Lütjering [10] described the important parameters of these four steps. For step I, the cooling rate from the homogenization temperature determines the width of the α-lamellae in the lamellar structure within the β grains and the extent of the continuous α-layer

at β grain boundaries. Although the homogenization temperature is kept low, and the homogenization time as short as possible, the β grain size is always fairly large (≥500 μm). By the step II, to introduce enough dislocations, preferably high amounts of plastic deformation is applied in the α + β phase field for obtaining complete recrystallization of the α and β phases during step III. And during the deformation process, crystallographic textures in the hexagonal α phase and in the bcc β phase can develop. The texture type depends on the deformation temperature. If the deformation temperature is low, which means high volume fraction of α phase is present, an α-deformation texture develops, and if the temperature is high, which means high volume fraction of β phase presents, a β-deformation texture develops. Also, there will be no significant change occurs in the textures of the hexagonal α during recrystallization.

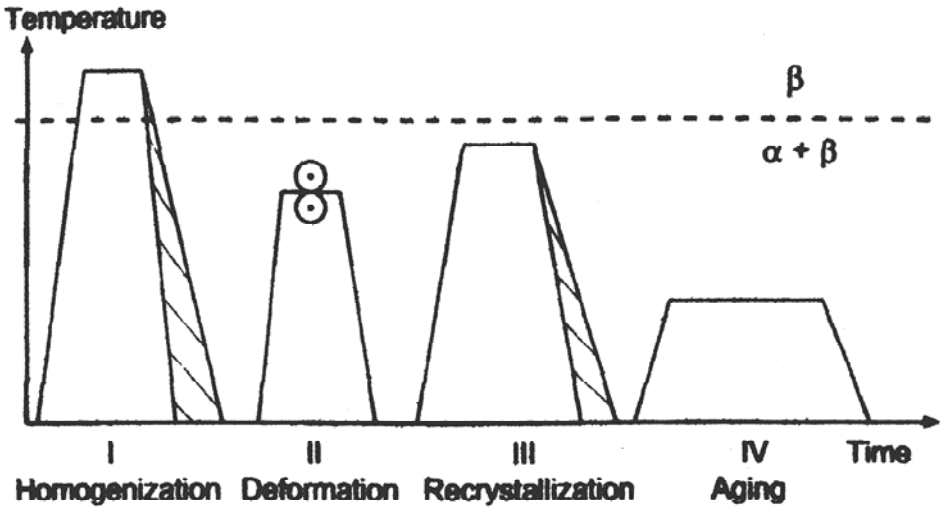



**Figure 2.6** – Processing route for bi-modal (duplex) microstructures [10].

For recrystallization step III, the temperature and the cooling rate from the recrystallization temperature are important parameters, which determines the volume fraction of recrystallized equiaxed $\alpha_p$ located at the "triple-points" of the recrystallized equiaxed β grains and the width of the individual α lamellae as well as the α colony size of the lamellar structure formed during cooling within the equiaxed β grains, respectively. If the cooling rate from the recrystallization

temperature is sufficiently low, no α lamellae are formed and only the $\alpha_p$ grains will grow within the β grains resulting in a so-called globular structure with the equilibrium volume fraction of β grains located at the “triple-points” of the α grains. The maximum α colony size is limited by the β grain size, which is the combination of $\alpha_p$ volume fraction and $\alpha_p$ size [10].

The effect of alloy element partitioning upon separation into $\alpha_p$ and β, the α lamellae formed during cooling from the β phase have a lower concentration of elements (especially oxygen), which are promoting age-hardening by formation of coherent $Ti_3Al$ particles in aging step IV. In this step, temperature is more important that time because the occurrence of the $Ti_3Al$ particles depends on the being either below or above the $Ti_3Al$ solvus temperature [10].

Lütjering [14] explained the main differences of bi-modal microstructure and the lamellar structure as the limited α colony size and the maximum length of α-lamellae as well as the effective length of grain boundary α-layers by small β grain size. The lamellar grains in the bi-modal structure are softer than the fully lamellar structure.

When the cooling rate increases, which is higher than a furnace cool treatment, the α colonies become progressively smaller, exhibit fewer platelets, and appear to nucleate independently of the β grain boundaries. The characteristic microstructure, “basket-weave” structure, forms by the distribution of these smaller colonies over all possible variants of the Burgers orientation relationship [4, 25].

During decomposition of β phase by a diffusionless process, known as martensitic transformation, α' martensite forms, which is a metastable fine plate-like, or acicular microstructure, at temperatures below $M_s$. Different types of martensite may form, hexagonal α' martensite or orthorhombic α" martensite, depending upon the alloy chemistry and the quenching temperature. Some retained β may also be present in the structure because of the martensite end

temperature, $M_f$, which is below room temperature (25 $^oC$). For Ti-6Al-4V, because V is a β stabilizer, the addition of 4% V to a Ti-6% Al alloy is sufficient to place the $M_f$ below room temperature. Thus, upon quenching, some β phase may not be converted to α' or α". Because the α' martensite has a similar orientation relationship to β as that of α, the martensitic microstructure is therefore also characterized by a very fine basket-weave structure with needle-like character due to its diffusionless nucleation process [1, 5, 11]. These results were consisted with the work of Malinov et. al. [9]. They also obtained α' martensite and no retained β phase during fast cooling conditions above from transus temperature in Ti-6Al-4V alloy system and quenching from 850 $^oC$ and continuing with aging between 600 and 700 $^oC$ gave them small changes in the diffraction pattern which were orthorhombic martensite (α"). Although the intensities of the α" martensite reflections were increased while increasing the treatment time at these temperatures, this microstructure were not seen at higher temperature (800, 900, 1000 $^oC$) treatments. Zeng and Bieler [19] reported the decomposition of α' martensite into α" during aging as decomposition of β phase precipitated from the decomposition of α' martensite into the α" and $\beta_{rich}$ phases. The transformation of α' into α" and β was thermodynamically unfavorable, because of the higher principle lattice strain between α' and α" than between α' and α due to the small lattice difference between α' and α phases, they described the transformation as written above. And after one year natural aging, they could not observe the appearance of α" and β phases which were all transformed into α. Also at the beginning of the experiments (quenching from 920 $^oC$), they had no α" martensites or retained β phases which were found from the TEM and X-ray analysis.

Similar to Malinov et. al. study [9], Jovanović et. al. [25] did not observe retained β phase upon fast cooling conditions with an exception at 1050 $^oC$ quenching case. In this case, the presence of small amount of the β phase was detected in the diffractogram and this was explained due to the lower values of martensite finish temperature for this alloy. According to the X-ray analysis, a decrease in the annealing temperature caused a decrease in the intensity of α'

martensite reflections indicating the decrease of the α' fraction, whereas an increase in the amount of the primary α phase.

Filip and his friends [27] had studies on the aging of the metastable phases which had effects on the mechanical properties. They showed that at higher ageing temperatures, the process of metastable phase decomposition became faster and the size of α lamellae colonies and the thickness of α-lamellae was increased and growth of equiaxial α phase grains took place.

### 2.4 Oxidation and Corrosion

Titanium and its conventional alloys have a tetragonal rutile crystal structure $TiO_2$, which is called scale, as an oxidation product during air exposure. This oxide layer is a thick, usually poorly adherent, an n-type anion-defective oxide through which the oxygen ions can diffuse. The solid solution significantly hardens the material and able to improve the wear resistance of titanium alloys [29]. The scale therefore grows into the base metal, which for example prevents the self-healing of cracks in Ti. The high chemical affinity between Ti and oxygen is the driving force for the rapid oxidation. During oxidation, the maximum solubility of oxygen in Ti of about 14.3wt.% and high chemical affinity results the formation of the scale and an α-case that is highly oxygen enriched adjacent inner layer in the base metal [4]. This layer was also seen in the study of Malinov et. al. [9], as a surface oxide layer, consisting of coarse α phase lamellae. Additionally, some coarse α phase colonies were grown towards the sample core. By using X-Ray measurements, they found that the oxide layer was growing with time and increasing its thickness during isothermal exposure at 600 $^{o}$C and also the microhardness values were measured 0.5 times larger than the matrix. Borgioli et. al. [29] found that hardened surface layer of Ti-6Al-4V alloy consists of an outer compound layer and an inner diffusion layer, after furnace treatments at varying times and temperatures. Treatments at 700 $^{o}$C showed that the compound layer has $TiO_2$ and small amounts of $TiN_xO_y$ and at higher temperatures, 900 $^{o}$C, poorly

adherent compound layer formed which has $Al_2O_3$ in the outer layer and $TiO_2$ and small amounts of $TiN_xO_y$ in the inner part. The diffusion layer consists of a solid solution of interstitial atoms in α – Ti. Also, at 900 $^oC$, they found that at the compound layer - diffusion layer interface, the intermetallic phase, $Ti_3Al$ is present. At higher temperatures, the application of conventional Ti – alloys is limited to the regime below about 550 $^oC$ where the low diffusion rates through the oxide layer prevent dissolved excess oxygen content in the bulk material. At temperatures above about 550 $^oC$, the material should be heated either in vacuum or in a protective atmosphere [4].

In order to decrease the diffusion rate of oxygen through the scale, the addition of elements with a valency greater than 4, such as $Nb^{+5}$, which can substitute the $Ti^{+4}$ ions in the $TiO_2$ structure, reduces the number of anion vacancies. Another effective method for lowering the diffusion rate is, increasing the amounts of Al to form α-$Al_2O_3$ oxide, which is very dense and thermally stable, results a heterogeneous mixture of $TiO_2$ and $Al_2O_3$ underneath a $TiO_2$ surface oxide. But for to this even higher concentrations of about 57 at.% Al would be required [4].

For the corrosion behavior point of view, because of having a stable and tightly adherent protective oxide layer on their surfaces, which resists the reaction between the metal or metal alloy and its environment by electron transfer from one species to another, titanium and its alloys are the most common materials used in biomaterial industry at the engineering level. Biocompatibility of these materials, like stainless steel, cobalt – based alloys, chromium and nickel – based alloys, are higher in vivo applications. So, titanium alloys have a great role, not only in implant industry, but also in aerospace and military industries because of their good mechanical properties with the addition of excellent resistance to corrosion [2, 4, 30].

Although titanium is chemically reactive, this thin oxide film passivates the base metal, as long as its integrity can be maintained. In most of the oxidizing

environments such as salt solutions, including chlorides, sulfates and sulfides or in nitric acid solutions, titanium and its alloys can exhibit resistance to corrosion. But under reducing conditions, the protective nature of the oxide film diminishes [2, 4].

The important mechanical properties and outstanding resistance to corrosion of the titanium and its alloys attracts scientists to work on them. Song et. al. [31] showed that in acidic solutions, the alloy composition had a significant influence on the anodic oxidation behavior of Al-Ti alloys. They observed that the formation rate of the oxide increased with the addition of aluminum up to a point and decreased for further increase, and additionally, they suggested that the lower electrolytic solution temperature should have been chosen. The evaluation of the electric field and the kinetics of the anodic oxide film was studied in Ti-6Al-4V ELI in NaCl solution which was formed potentiostatically by Nowak and Sun [32]. They explained that the formation of the film occurred under a constant electric field and observed that during its growth, the decrease and the increase of the potential drop was balanced at the rate determining interface and through the film, respectively. Robin et. al. [33] had studies on the Ti-4Al-4V alloy in different acid solutions at room temperature and examined that solutions other than containing 40% - 80% $H_3PO_4$ and $H_2SO_4$, did not have significant effects on corrosion behavior of the alloy, although the dissolution of aluminum from the passive film was seen after long term immersion tests. The differentiation of the element content in the passive film from the base metal and the chemical composition variation of the film due to the solution composition were shown as a reason of different passive film behavior. Other than the previously discussed studies, Aziz-Kerrzo et. al. [34] examined the pitting initiation at the surface of Ti-45Ni alloy in saline-buffered solution while that was not seen in pure titanium or Ti-6Al-4V alloy. They also observed that the films, which were seen in these three alloys, were analyzed in terms of a dual oxide layer comprising an inner barrier and an outer porous layer. Also, the dependence of the porous layer with the nature of the alloy and the solution anion species was found. By using different solution, which were included halide anions mostly, pitting corrosion of

$Ti/TiO_2$ was determined by Basame and White [35]. Their results indicated that the chemical nature and concentration of anions in the solution determined the pitting corrosion; especially $Br^-$ anion included one than $I^-$ or $Cl^-$ ones. The correlation between electrochemical activity and pitting corrosion was explained as an increase in the electric field within the oxide layer because of local film thickness decrease in these areas resulting an electron tunneling across the film. During evaluation of the pitting corrosion resistance of the materials, the pitting potential is considered as a criterion. As discussed in the previously mentioned study [36], the pitting potential of an alloy is directly influenced by the amounts of passivating elements present in the alloy. Morris [37] and Mudali et. al. [38] explained that the direct measure technique of the pit propagation kinetics could be found by the hysterisis loop in the cyclic polarization curve and the pit protection potential was given as the intersection point of the reverse scan and the sweep direction of the polarization curve.

The recent studies, which have been using simulated body fluids for corrosive environment, have given information about the corrosion behavior of biomaterials. Gurappa [39] reported the importance of the biomaterials and why the titanium and its alloys were important in biomedical applications. According to his results, obtained from 2 different biomaterials other than CP-Ti and Ti-6Al-4V, he concluded that because of the corrosion resistance in tissue, absence of tissue toxicity and allergic reactions, and good mechanical properties titanium and its alloys were mostly chosen for biomedical applications. Not only comparison of other materials were studied but also different surface treatments with varying solutions have tried for several years in the titanium and its alloys. Cai et. al [40] worked on the commercially pure titanium which had been given different surface conditions after casting of the material. At 37 $^oC$, specimens were tested in artificial saliva and acidic saline solution by potentiodynamic anodic polarization after long term immersion period. Their results showed that the surface roughness significantly affected the polarization behavior of the CP titanium and addition to the surface roughness, surface reaction layers had also effect on the dissolution of titanium into the test solution. Another study of Cai et. al. [41] sandblasting was

said to be a more rigorous process than polishing. Their studies on the different cast titanium alloys exhibited, as similar in the previous study [40], marked effect of surface preparation on the corrosion of the alloys. The alloying elements effect and their dissolution into the solution were also the main points of the works of Kuphasuk et. al. [42], Ibriş and Rosca [43], and Choubey et. al. [44]. Ibriş and Rosca, and Choubey et. al. were done their studies in Ringer's solution and Hank's solution at 37 $^{o}$C, respectively. Kuphasuk et. al. [42] worked on six different titanium alloys by scanning their voltages potentiostatically. They discussed that no alloy element dissolution was observed other than Ni and applied potentials were reached at a point which were all higher than the NiTi alloy system due to the stability of titanium oxide film. Therefore, pitting corrosion was only seen in NiTi alloy system. Ibriş and Rosca [43] were chosen Ti, Ti-7Al-4.5V, and Ti-5Al-2.5Fe for their experiments by using Electrochemical Impedance Spectroscopy (EIS). Their investigation showed that the influence of the alloying element is reflected, especially for the iron-containing alloy, mainly in an increasing oxide resistance and growth rate by enhancing the diffusion of $Ti^{+3}$ ions, but no effect on the charge transfer reaction. Similar to the alloy systems used in [42], Choubey et. al. [44] used 8 different Ti-based alloys but in this case potentiodynamic polarization was chosen. They showed that the substitution of Fe in place of V did not affect the corrosion rate and contrary to the discussion in [31], addition of only Al to Ti (15wt%) was detrimental to the passivity of Ti. The specimens were also inspected microscopically and mostly the amount of β phase was taken into consideration. At this point of view, Ti-13Nb-13Zr was said to exhibit low corrosion rates due to the maximum fraction of beta phase. This was also consistent with Lopez et. al. [45] study. They discussed that the observed passive layer was very protective because of the diffusion of the Al and Zr towards the surface from the bulk. Inversely, Ti and Nb were found more in the bulk than the surface. So, the higher concentration of Al and Zr in the passive layer was given as the reason of lower current densities. They also observed that the alloys, which included more Nb and Zr alloying elements, did not show any breakdown potential in any case. Therefore, the susceptibility to pitting corrosion is very low with respect to the other Ti-alloys.

The Nb effect in place of V on the corrosion behavior was reported in details in Metikoš-Huković et. al. [46] study. They discussed that presence of vanadium in the oxide of titanium might cause an increase in the concentration of defects and a decrease in corrosion resistance, which was not seen in Nb because of radii similarity of Ti and Nb with respect to V. Additionally, vanadium oxide dissolution from the oxide layer in Ti-6Al-4V, due to the $Cl^-$ ion adsorption from the solution, caused an increase in the localized corrosion susceptibility of the alloy. Mareci et. al. [47] investigated again different types of titanium alloys, only Ti-6Al-4V had the vanadium for β stabilizing element. They tried varying immersion time scales for the passive film formation in artificial saliva and scanned them potentiodynamically, and found that although polarization over + 800mV exhibited smallest current densities, Ti-6Al-4V had the highest corrosion rates than all other titanium and titanium alloys.

Similar studies about passive film dissolution and pitting formation were also done in simulated human body solutions. Al-Mayouf et. al. [48] worked on the alloys which were used in dental applications in artificial saliva at different pH values and $F^-$ ion concentrations, and reported, by using open-circuit potential and polarization resistance techniques and EIS method, that lower pH values hindered the formation of a protective layer and corrosion even in low fluoride concentrations occurred, which were not observed in neutral conditions. In pitting corrosion, the effect of temperature was investigated by Burstein et. al. [49]. They showed that the frequency of breakdown was very low at ambient temperature but increased with increase in temperature. Their results were consistent with the study of Metikoš-Huković et. al. [46], in which chloride ion migration across the film was the reason of pit nucleation that was the result of the accumulation of metal chloride at the metal/film interface.

The formation of passive oxide layer during electrochemical processes also depends on the microstructural developments in the working material. The effect of phase transformation during film formation was the main point for some of the scientists. Sittig et. al. [50] investigated the different oxide film formations on the

α and the β phases in Ti-6Al-7Nb by several methods. For clear observation, the specimen was annealed at 900 $^{o}$C for 4 hours in air to increase the grain size of the both phases. By X-ray photoelectron spectroscopy and scanning Auger microscopy exhibited that aluminum was enriched above the α phase and niobium above the β phase. Although lateral force measurements indicated slight differences in the pH-dependence of the frictional force on the two oxide phases, on α phase higher friction was observed than the β phase. Another heat treated titanium alloy was studied by Greetha et. al. [51]. They used Ti-13Nb-13Zr alloy for their experiments and the measurements were accomplished in Ringer's solution. They obtained martensitic microstructure by quenching from the β solution temperature and acicular α by furnace and air cooling and aging was done for 4 hours. They obtained α', α", α and β in the microstructures and worked on the effect of these on the corrosion behavior. They obtained that fast cooling from β solutionizing temperature and aging exhibited the lowest passive current density amongst others. The passive current density increase was explained due to the depletion of the alloying elements Zr and Nb in α phase. This is consistent with the Metikoš-Huković et. al. [46] that Nb is said to be beneficial due to annihilation of anion vacancies in the crystal lattice of titanium. Additionally, the aging of α + β solutionizing and water quenching resulted in the formation of a stable oxide layer according to the homogeneous distribution of the alloying elements during heat treatment. And also they concluded that all the air cooled specimens exhibited active open circuit potential (OCP) and high passive current density. On the other hand, microstructure was investigated by using different solutions as used in Bearinger et. al. [52] and Codaro et. al. [36] which were phosphate buffered solution (PBS) and NaCl solutions, respectively. Bearinger et. al. examined the dome (structure of an oxide formed on the grains for a given microstructure) growth on the grains in CP-Ti and Ti-6Al-4V by using Atomic Force Microscopy (AFM) and Step Polarization Impedance Spectroscopy (SPIS). They observed the dependence of initial oxide growth processes on time and voltage, and gave an explanation to the electrical independence of the hydration of the titanium surface because of titanium oxide's n-type semiconductor

classification. Differently, the pitting corrosion and the size and distribution of the pits on the surface of Ti-6Al-4V was the important parameters in Codaro et. al. work. Similar in Bearinger et. al. [52] and Codaro et. al. [36], they followed a heat treatment sequence, which were α + β annealing and furnace cooling, and quenching from β solutionizing temperature and aging, to maintain different microstructures. Their results exhibited that both microstructure and corrosive media had specific influences on pitting. They classified the pit formation conditions and explained that aged specimens had been affected at most. And they used not only NaCl immersion test, but also Salt-Spray testing to obtain more attacked surfaces for classification.

# CHAPTER 3

## BASICS OF CORROSION

### 3.1 Introduction to Corrosion

Corrosion is a degradation or destruction of a metal by means of a chemical or electrochemical reaction with its surrounding environment that produces a deterioration of the material and its properties [2, 30]. Determining the capacity of materials to resist deterioration without modifying their surface and bulk initial properties, when exposed to aggressive media during service, is one of the important pieces of information required at the moment of selecting a material for a given application. So, to determine whether a material can be considered as resistant to corrosion, corrosion science and engineering offers methods and characterization techniques which include the study of the chemical and metallurgical processes and the design and application of methods, respectively [2, 30]. The corrosion process involves two reactions: anodic and cathodic which are governed by the following equations:

| | | | |
|---|---|---|---|
| Anodic process: | $M \rightarrow M^{+n} + ne^{-}$ | Metal Oxidation | (3.1) |
| Cathodic process: | $nH^{+} + ne^{-} \rightarrow H_2$ | Hydrogen Evolution | (3.2) |
| | $O_2 + 2ne^{-} \rightarrow nH_2O$ | Oxygen Reduction | (3.3) |
| | $M^{+n} + ne^{-} \rightarrow M$ | Metal Reduction | (3.4) |

For corrosion to take place, both anodic and cathodic processes must be present. Corrosion processes are controlled both by thermodynamics and kinetics, which are about the fundamental feasibility of the reaction and the rate, respectively. The thermodynamic feasibility of a reaction can be calculated by using the intimately linked free energy change, $\Delta G$ and the electrochemical potential of a reaction, $E$ or $E_{corr}$, at equilibrium, with a relationship [2].

$$\Delta G = -nFE_{corr} \tag{3.5}$$

where n is the number of equivalents exchanged in the reaction, and $F$ is Faraday's constant, 96500 coulombs per equivalent. The electrochemical potential of a reaction, $E_{corr}$, is the algebraic sum of the half-cell reaction potentials of anodic and cathodic reactions, defined as $e_a$ and $e_c$, respectively. A positive $E_{corr}$ corresponding to a negative ΔG indicated that the reaction is spontaneous in the written direction. When determining the spontaneous direction of an electrochemical reaction, the $e_a$ and $e_c$ values are calculated according to the departures from standard half-cell electrode potentials at unit activity due to concentration changes by the Nerst Equation for a general half-cell reaction, given as [2];

$$aA + mH^+ + ne^- \rightarrow bB + dH_2O \tag{3.6}$$

$$e = e_o + \frac{2.3RT}{nF} \log \frac{(A)^a \left(H^+\right)^m}{(B)^b \left(H_2O\right)^d} \tag{3.7}$$

the 2.3 is ln(e) and converts from natural to base 10 logs.

### 3.2 Electrochemical Kinetics of Corrosion

Corrosion is thermodynamically possible of most environmental conditions. Thus, it is important to know how fast corrosion takes place. So, to develop more corrosion-resistant alloys and to improve methods of protection against corrosion, an understanding of the fundamental laws of electrochemical reaction kinetics is essential.

#### 3.2.1 Faraday's Law

The rate of electron flow to or from a reacting interface is a measure of reaction rate. The proportionality between current, $I$, in amperes, and mass reacted, $m$, in an electrochemical reaction is given by Faraday's Law [2];

$$m = \frac{Ita}{nF} \tag{3.8}$$

where $a$ the atomic weight, and $t$ the time. Dividing equation (3.8) through by $t$ and the surface area, $A$, yields the corrosion rate, $r$ [2];

$$r = \frac{m}{tA} = \frac{ia}{nF} \tag{3.9}$$

where *i*, defined as current density $(I/A)$. This equation shows a proportionality between mass loss per unit area per unit time (e.g., $mg/dm^2/day$) and current density (e.g., $\mu A/cm^2$). Units of penetration per unit time result from dividing equation (3.9) by the density, $D$, of the alloy. For corrosion rate in millimeter per year, equation (3.9) becomes

$$r = 0.00327\frac{ai}{nD} \text{ (in } mm/yr) \tag{3.10}$$

### 3.2.2 Electrochemical Polarization

Polarization, $\eta$, is the potential change from the equilibrium half-cell electrode potential, $e$, caused by a net surface reaction rate for the half-cell reaction. For cathodic polarization, $\eta_c$, because the electrons are supplied to the surface, and building up in the metal due to the slow reaction rate, the surface potential becomes negative to $e$. Hence, $\eta_c$ is negative. For anodic polarization, electrons are removed from the metal which results a deficiency in a positive potential change due to the slow liberation of electrons by the surface reaction, and $\eta_a$ must be positive [2].

#### 3.2.2.1 Activation Polarization

When some step is in the half-cell reaction controls the rate of charge flow, the reaction is said to be under activation or charge-transfer control, and activation polarization results. The relationship between activation polarization or overpotential, $\eta$, and the rate of the reaction represented by current density, $i_a$ or $i_c$, is [2]

$$\eta_a = \beta_a \log \frac{i_a}{i_o} \tag{3.11}$$

for anodic polarization, and

$$\eta_c = \beta_c \log \frac{i_c}{i_o} \tag{3.12}$$

for cathodic polarization. $\beta_a$ and $\beta_c$ are known as the Tafel constants for the half-cell reaction and $i_o$ is the exchange current density. The theoretical derivation of the above Tafel relationships (3.11) and (3.12), is as follows. Taking reaction (3.2) as an example, at equilibrium the rate of discharge of $H^+$ (forward) exactly

balances the rate of ionization of $H_2$ (reverse). The presence of overpotential suggests the presence of energy barriers (activation energies), $\Delta G_f^*$ and $\Delta G_r^*$, corresponding to the forward and reverse reactions, respectively, as shown schematically in Figure 3.1. The activation energy difference is related to the half-cell electrode potential by the expression [2];

$$\Delta G_f^* - \Delta G_r^* = \Delta G_{H^+/H_2} = -nFe_{H^+/H_2} \tag{0.1}$$

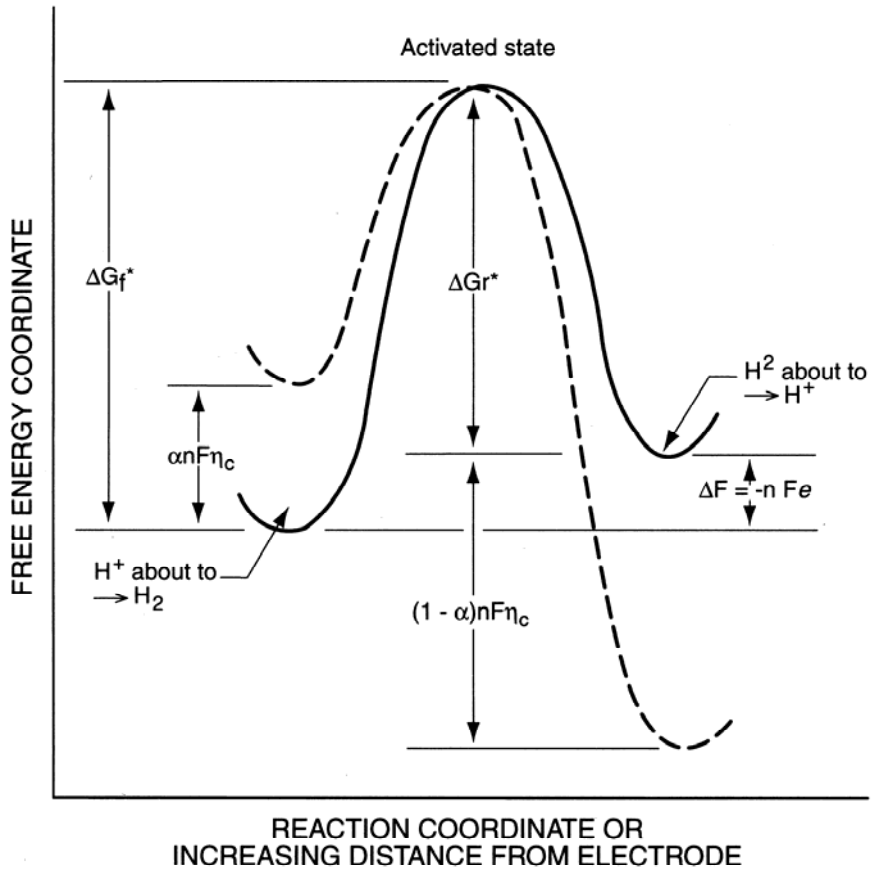



**Figure 3.1** Activation energy model for activation overpotential. Equilibrium state ( ——— ); polarized state ( - - - - - - - - ) [2].

The reaction rates as a function of the respective activation energies for forward, $r_f$, and reverse, $r_r$, reactions are [2];

$$r_f = K_f \exp\left[\frac{\Delta G_f^*}{RT}\right] \tag{3.14}$$

and

$$r_r = K_r \exp\left[-\frac{\Delta G_r^*}{RT}\right] \tag{3.15}$$

where $K_f$ and $K_r$ are the reaction rate constants, $R$ is a gas constant and $T$ is the absolute temperature. At equilibrium,

$$r_f = r_r = \frac{i_o a}{nF} \tag{3.16}$$

Thus,

$$i_o = K_f' \exp\left(-\Delta G_f^* / RT\right) = K_r' \exp\left(-\Delta G_r^* / RT\right) \tag{3.17}$$

When a cathodic overpotential, $\eta_c$, is applied to the electrode, the discharge reaction rate is reduced by an amount, $\alpha nF\eta_c$, and that of the ionization is increased by an amount $(1-\alpha)nF\eta_c$. The factors $\alpha$ and $(1-\alpha)$ are the fractions of $\eta_c$, where $\alpha$ is a constant related to the symmetry of the effects of a change in potential on the forward and reverse reaction rates, and is typically in the region of 0.5, respectively. Then the cathodic discharge reaction rate in terms of current density becomes;

$$i_c = K_f' \exp\left[-\frac{\Delta G_f^* - \alpha nF\eta_c}{RT}\right] \tag{3.18}$$

and the anodic ionization reaction becomes;

$$i_a = K_r' \exp\left[-\frac{\Delta G_f^* + (1-\alpha) nF\eta_c}{RT}\right] \tag{3.19}$$

Then the net applied current is given as;

$$i_{app,c} = i_c - i_a = i_o \exp\left[\frac{\alpha nF\eta_c}{RT}\right] - i_o \exp\left[\frac{-(1-\alpha) nF\eta_c}{RT}\right] \tag{3.20}$$

For an applied anodic current favoring ionization to $H^+$,

$$i_{app,a} = i_a - i_c = i_o \exp\left[\frac{\alpha nF\eta_a}{RT}\right] - i_o \exp\left[\frac{-(1-\alpha) nF\eta_a}{RT}\right] \tag{3.21}$$

where $\alpha$ is now the fraction of $\eta_a$ taken by the anodic ionization reaction. These equations are known as the Butler-Volmer equation [2]. For high values of $\eta_c$ and $\eta_a$ (several 100 mV), the equations (3.20) and (3.21) simplifies to

$$i_{app,c} = i_c - i_a = i_o \exp\left[\frac{\alpha nF\eta_c}{RT}\right] \tag{3.22}$$

and

$$i_{app,a} = i_a - i_c = i_o \exp\left[\frac{\alpha nF\eta_a}{RT}\right] \tag{3.23}$$

which are identical to

$$\eta_{act,c} = \beta_c \log\frac{i_c}{i_o} \tag{3.24}$$

and

$$\eta_{act,a} = \beta_a \log \frac{i_a}{i_o} \tag{3.25}$$

with $\beta = 2.3RT/\alpha nF$, respectively, where the Tafel coefficient, $\beta$, is related to the kinetics of the rate-determining step (RDS) of the reaction, and typically has a value of the form ($RT$ / $\alpha nF$) [2].

#### 3.2.2.2 Polarization Resistance, $R_p$

Polarization resistance, defined as the slope of the polarization curve at the origin, $\Delta E - \Delta I$, is independent of the degree of linearity. It has dimensions of ohms and is synonymous with "linear polarization" in describing the "Stern-Geary" technique for evaluating corrosion rates. Stern and Geary on the basis of a detailed analysis of the polarization curves of the anodic and cathodic reactions involved in the corrosion of a metal, and on the assumption that both reactions were charge-transfer controlled (transport overpotential negligible) and that the $iR$ drop involved in determining the potential was negligible [7]. When both polarizing them from the corrosion potential, $E_{corr}$ with cathodic and anodic applied current densities, $i_c$ and $i_a$,

$$\varepsilon_c = \beta_c \log \frac{i_c}{i_{corr}} \tag{3.26}$$

and

$$\varepsilon_a = \beta_a \log \frac{i_a}{i_{corr}} \tag{3.27}$$

where $\varepsilon_c$ and $\varepsilon_a$ are the cathodic and anodic overvoltages, $\beta_c$ and $\beta_a$ are cathodic and anodic Tafel constants (activation polarization), respectively, and $i_{corr}$ is the corrosion rate as current density. $\varepsilon_c$ and $\varepsilon_a$, which are to be distinguished from overvoltages previously designated by $\eta$, are defined as potential changes from the steady-state corrosion potential. By converting equations (3.26) and (3.27) to exponential form and subtracting them similarly in equation (3.20), we obtain;

$$i_{app,c} = i_{corr}\left(10^{-\varepsilon_c/\beta_c} - 10^{\varepsilon_a/\beta_a}\right) \tag{3.28}$$

As $\varepsilon \to 0$, the difference between two exponential functions, $i_{app,c}$, approaches linearity with overvoltage $\varepsilon$. And rearrangement of above equation and differentiation gives the polarization resistance, $R_p$ [2];

$$R_p = \left[\frac{d\varepsilon}{di_{app}}\right]_{\varepsilon\to 0} = \left[\frac{\Delta E}{\Delta i_{app}}\right]_{\varepsilon\to 0} = \frac{\beta_a\beta_c}{2.3i_{corr}\left(\beta_a+\beta_c\right)} = \frac{B}{i_{corr}} \tag{3.29}$$

Thus, the slope, $\left(d\varepsilon/di_{app}\right)_{\varepsilon\to 0}$, at the origin of the polarization curve, defined as polarization resistance, $R_p$, is inversely proportional to the corrosion rate where

$$B = \frac{\beta_a\beta_c}{2.3\left(\beta_a+\beta_c\right)} \tag{3.30}$$

is the proportionality constant which is known as Stern and Geary coefficient [53]. Equation (3.29) shows that the corrosion rate is inversely proportional to $R_p$ (or directly proportional to the reciprocal slope of the $\Delta E - \Delta i$ curve) at potentials close to $E_{corr}$, and at that $i_{corr}$, can be evaluated providing the Tafel constants are known.

### 3.3 Passivation

Passivation is caused by formation of a thin, protective, hydrated oxide, corrosion product surface film that act as a resistive barrier between the solution and the metal, and leads to a marked reduction in the rate of the anodic reaction. In simple terms the rate of the anodic reaction in steady-state conditions will be the rate of dissolution of the passive film. The passive current density, $i_{corr}$, which is the rate of the anodic reaction in the passive region, is usually relatively independent of potential, since it is controlled by the rate of dissolution of the passive film. Where there is a region of solubility of the corrosion product between the region of stability of the metal and of the passivating oxide film, then an *active-passive transition* will be observed. At potentials just above the equilibrium potential for the metal, the metal will corrode actively, and activation kinetics will apply. As the potential moves up into the region where the passive oxide film is stable, then the surface will passivate, and the current will fall rapidly to the passive current density [2].

When the potential exceeds the equilibrium potential, the oxygen evolution reaction starts to occur on the surface of the passive film. The rate of this reaction will depend on the electronic resistance of the passive film (since electrons must pass through the film to permit the oxygen evolution reaction to occur) and on its electrochemical reactivity. If the metal oxide can be further oxidized to a more soluble state, transpassive (meaning 'above passive') corrosion can occur [2].

If the metal is susceptible to localized corrosion, local breakdown of the passive film can occur, leading to pitting corrosion, crevice corrosion, and embrittlement by stress corrosion cracking.

# CHAPTER 4

## EXPERIMENTAL DETAILS

### 4.1 Material and Specimen Preparation

The material that was used in this study was Ti-6Al-4V ELI (Extra Low Interstitial) type titanium alloy and the standard chemical composition of the alloy is given in the Table 4.1.

**Table 4.1** The chemical composition of Ti-6Al-4V ELI alloy [54].

| Component | Al | C | Fe | H | N | O | Ti | V |
|---|---|---|---|---|---|---|---|---|
| Wt% | 5.5-6.5 | Max 0.08 | Max 0.25 | Max 0.0125 | Max 0.05 | Max 0.13 | 88.1-91 | 3.5-4.5 |

The heat treatment procedures that were applied to obtain different microstructures were summarized in Table 4.2. For physical characterization of the microstructure and corrosion tests two samples were treated identically.

The heat treatments were carried out in a vertical tube furnace under argon atmosphere. Before the lowering of the samples to the hot zone of the furnace, argon gas was flushed several times in order to reduce the oxygen content of the furnace. The solutionizing temperature and time was 1060 $^{o}$C and 20 minutes, respectively. As the quenching medium, the mixture of ice, 30 gr salt and 30 ml alcohol is used which maintains -18 $^{o}$C temperature.

**Table 4.2** Heat treatments of Ti-6Al-4V ELI.

| Name of the specimen | Heat treatment time and temperature |
|---|---|
| FC | Solution annealed at 1060 $^{o}$C for 20 min + furnace cool |
| AC | Solution annealed at 1060 $^{o}$C for 20 min + air cool |
| WQ | Solution annealed at 1060 $^{o}$C for 20 min + water quench |
| WQ-500 | WQ + aging at 500 $^{o}$C for 10 hr + air cool |
| WQ-600 | WQ + aging at 600 $^{o}$C for 10 hr + air cool |
| WQ-700 | WQ + aging at 700 $^{o}$C for 10 hr + air cool |
| WQ-800 | WQ + aging at 800$^{o}$C for 10 hr + air cool |
| WQ-900 | WQ + aging at 900 $^{o}$C for 10 hr + air cool |

The specimens used in the experiments are cylindrical in shape having 10 mm length and 12 mm diameter. The specimens were put into stainless steel crucibles and covered with pure titanium powder and also sacrificial Ti-6Al-4V discs were placed on top of the crucibles for further prevention of specimen from oxidation. Then the regarding heat treatment was applied to specimens. The all heat treated specimens were ground by 80 to 1200 grit emery paper and also polished 1μm alumina paste for shining appearance. One sample in the set of specimen was prepared for X-Ray analysis, Scanning Electron Microscopy (SEM) analysis and hardness measurement; and other one was prepared for corrosion measurements.

X-ray analysis was carried out on the heat treated specimens by using Rigaku D / Max 2200 / PC model X-Ray Diffractometer. Diffractograms were obtained by continuous scanning at 40 kV / 40mA between 25$^{o}$ to 90$^{o}$ 2θ angles with 0.01 step size. The determination of cell parameters for the hexagonal ($P6_3/mmc$ spg) α phase was made by using these diffraction patterns for all heat treated specimens. Firstly, the 2θ and *hkl* parameters of (004) peak was used in order to calculate "c" value according to the equations (4.1) and (4.2) below which are the Bragg's Law and interplanar spacing equation for *hkl* in HCP structure, respectively. Secondly,

by using the (202) peak in the diffraction pattern, the "a" value was obtained by inserting the "c" value into the same equation (4.2) and repeated it for all heat treatment conditions. Also, by using the data, which was discussed above, the "c/a ratio" and the "unit cell volume" were calculated for α phase.

$$\lambda = 2d_{hkl} \sin\theta \tag{4.1}$$

$$\frac{1}{d_{hkl}^{\,2}} = \frac{4}{3}\left(\frac{h^2 + hk + k^2}{a^2}\right) + \frac{l^2}{c^2} \tag{4.2}$$

where $\lambda$ is wavelength, $\theta$ is Bragg angle and $d_{hkl}$ is interplanar spacing for $hkl$.

The microstructural characterization was made by SEM using JEOL JSM-6400 Electron Microscope and the spectral analysis was done by NORAN System SIX X – Ray Microanalysis System with Energy Dispersive Spectrometry (EDS) technique. The specimens were etched by 6 ml $HNO_3$ + 3 ml HF + 100 ml deionized water solution, known as Kroll's reagent.

After X-Ray and SEM analysis, hardness was measured by using Heckert Analogue Hardness Machine with Brinell intender under 62.5 kg constant load. Before the hardness experiments specimens were embedded in bakelite to obtain a rigid foundation.

The specimens, for corrosion experiments, firstly drilled on one side of the 10 mm long samples and secondly, in order to have mechanical contact, cupper wires were soldered to the drilled hole. After that specimens were molded in polyester resin to form a flat cross sectional area. Therefore, only the surface of the specimen interacts with corrosive medium. Specimens were then prepared metallographically using 80 to 1200 grid emery papers and two step polishing were done by 1μm and then 0.3 μm alumina paste to obtain shiny appearance. Finally, specimen surfaces rinsed by water and then with alcohol and dried in fan air.

The corrosion experiments were carried out in 1L Ringer's solution, where pH 7.2, and in Ringer's solution with 0.1M and 0.2M NaF at 37 $^{o}$C in a thermostated water bath with ±0.1 $^{o}$C accuracy, where the chemical composition of the solution is given in Table 4.3. The test solution is prepared freshly with stirring and used not more than four times due to possible breakdown of solution purity.

**Table 4.3** The chemical composition of the Ringer's Solution.

| **Name of the compound** | **Weight of the added compound** |
|---|---|
| NaCl | 9 gr |
| $CaCl_2$ | 0.24 gr |
| KCl | 0.43 gr |
| $NaHCO_3$ | 0.2 gr |
| Deionized water | 1000 ml |

## 4.2 Experimental Procedure

### 4.2.1 Open Circuit Potential (OCP) Measurement

The open circuit potential measurements were made, using a 4.5 digit digital voltmeter, against stainless steel counter electrodes in Ringer's solution and in Ringer's with 0.2M NaF, which is maintained at 37 $^{o}$C for four days in a thermostated water bath.

### 4.2.2 Anodic Polarization Measurement

The electrochemical polarization cell is a 1 L flask and a Teflon lid with four openings for working and counter electrodes, thermometer, and reference electrode. In this design, the specimen with flat surface is positioned at one side of the flask facing the platinum counter electrode.

The potential of the working electrode is measured by means of reference electrode. This is achieved with using the luggin probe, which is flexibly mounted to the flask and probe tip was placed near the specimen surface to minimize $IR$-drop. But because of the electrolyte solution conductivity, the probe tip cannot be placed too close less than 1 mm [2]. The electrolyte is carried between the reference and working electrode by the salt bridge. The saturated calomel electrode is used as reference electrode, which is positioned in a salt bridge. Saturated calomel reference electrode is composed of $Hg_2Cl_2$, mercury and saturated potassium chloride solution and also platinum wire provides electrical connection into corrosion cell. The specimen, counter electrode and a calomel reference electrode are connected to Solartron 1480 Multi Channel potentiostat. The potentiostat is controlled by Corrware software, which enables the control of the test parameters to be specified and the results to be implemented.

Anodic polarization measurements were done for two different specimen conditions. First one is the initially passivated specimen for 4 days under open circuit condition, and the second is the fresh and polished surface condition. For the first surface condition, voltage was scanned anodically from 0.5 V below $E_{corr}$ to 3,5 V vs SCE with the scan rate of 1 mV/sec. For the second surface condition, anodic scan has been started from -1.5 V below $E_{corr}$, in order to remove any possible oxide layer, to 3 V vs SCE with the same scan rate. The data acquisition for the experiments was 1 pt/sec. The test solutions were similar, Ringer' solution and 0.1M and 0.2M NaF added Ringer's solution. The polarization curves were then examined to determine passivation potentials, $E_{pas}$, current densities, $I_{pas}$, corrosion potential, $E_{corr}$ and corrosion current density, $I_{corr}$.

To determine corrosion rates of the specimens, polarization resistance technique was used. For this purpose a computer program has been written to process the experimental data. In this program, firstly, $I$ vs $E$ data was spline fitted in the range from ±10 mV around the corrosion potential, $E_{corr}$. Then the root of the spline curve was calculated where the corresponding potential is the

corrosion potential. After that, again with the same range, $I$ vs $E$ data this time was fitted to a line where the reciprocal of the slope gave the polarization resistance, $R_p$.

As can be seen in equation (3.29), corrosion potential can be evaluated from $R_p$ if Stern – Geary coefficient, equation (3.30), is known. Therefore, in order to calculate $B$, the approach suggested by Mansfeld [55] was used. In this approach, $I_{corr}$ in Butler-Volmer equation, equation (3.20), was substituted by $B/R_p$, giving that [7];

$$I = \frac{B}{R_p}\left\{\exp\left(\frac{2.3\left(E-E_{corr}\right)}{\beta_a}\right)-\exp\left(\frac{-2.3\left(E-E_{corr}\right)}{\beta_c}\right)\right\} \tag{4.3}$$

where $B=\beta_a\beta_c/2.3\left(\beta_a+\beta_c\right)$, $\beta=2.3RT/\alpha nF$ and $\eta=E-E_{corr}$ for equation (3.20). This equation was then optimized, using principal axis minimization method, with respect to $\beta_a$ and $\beta_c$ for every point in the data set. So that experimental $I$ and theoretical $I$ in equation (4.3) agrees each other with minimum error. Generally the agreement we have found between equation (4.3) and experiment was very good where the order of error is around $10^{-7}$. Then using Tafel constants, $B$ was evaluated and $I_{corr}$ can be found by equation (3.20).

Finally, the corrosion rates in (mmPY) was evaluated using [2]

$$Rate=\frac{0.00327\left(eqw\right)10^6 I_{corr}}{D} \tag{4.4}$$

where $eqw$ is equivalent weight in gr, 0.00327 comes from unit conversion of time parameter $I_{corr}$ is corrosion current density, $D$ is density in gr/cm$^3$.

# CHAPTER 5

## RESULTS AND DISCUSSION

### 5.1 Microstructural Examinations

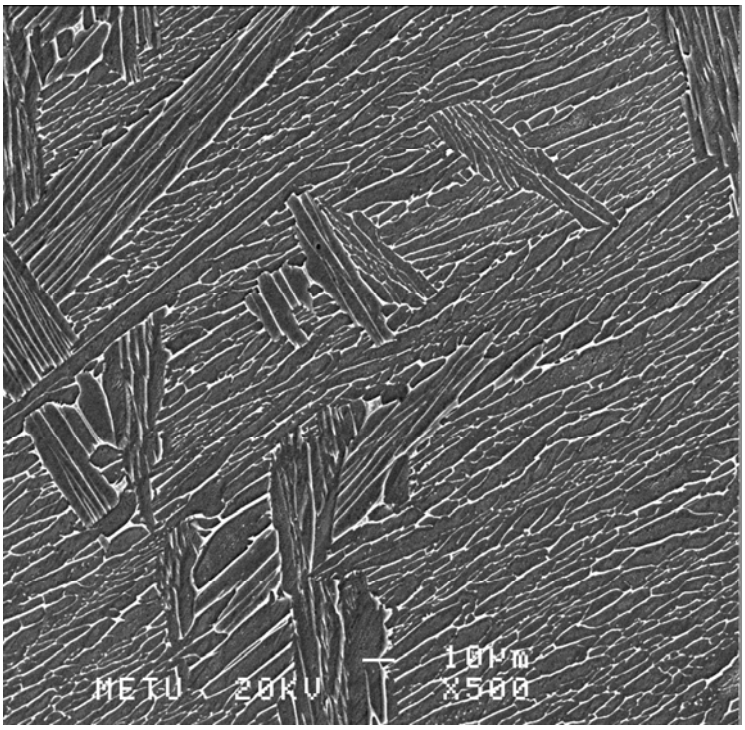
The heat treatments which were applied to the Ti-6Al-4V ELI alloy exhibited different microstructures. These microstructures were morphologically examined and chemical compositions of the phases were taken by using SEM. All of the taken SEM photographs were given in the below Figures 5.1(a-h). In the SEM images, the dark and the white regions were identified as α and β phases, respectively.

In the Figure 5.1(a), the equilibrium α and β phases, which were obtained by furnace cooling from 1060 $^{o}$C, can be seen. In this heat treatment, the α phase is named as Widmanstätten α and morphologically it is not only continuously lined up, but also nucleated inside pre-existing β grain during cooling from β solutionizing temperature, and β phase is also continuously formed parallel to the α phase. α phase was firstly nucleated on the grain boundaries of the β grains and grown towards the inside of the grain. During cooling, nucleation inside the grain might also be effective so continuity of the columnar α phase was prevented by itself. In this microstructure, the alloying element composition of the α and β phases were detected as 2.09wt% V and 6.72wt% Al for α phase (dark region), and 10.53wt% V and 3.63wt% Al for β phase (white region).

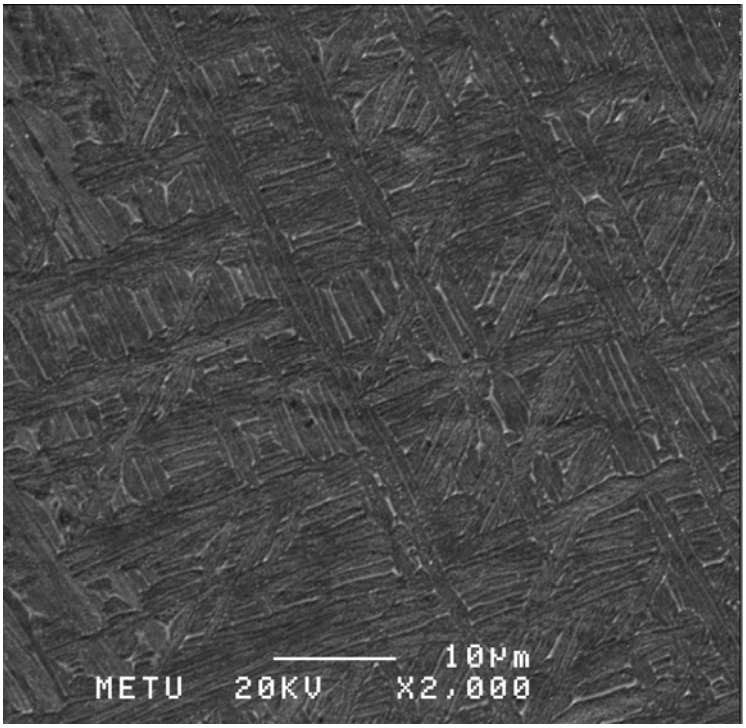
In Figure 5.1(b), the microstructure of the air cooled specimen, which is intermediate cooling between furnace cooling and water quenching, was given. The heat treatment resulted in equilibrium α phase as in furnace cooling but less β

phase in this case and the obtained structure of the α phase is known as basket-weave α. The compositional variation throughout the microstructure could not be determined precisely with EDS analysis technique used in the investigations, so no composition analysis was given for AC.

The fastest cooling rate from β transus temperature exhibited martensitic transformation as seen in Figure 5.1(c). The obtained microstructure is known as α'-martensite and the chemical composition of this kind of heat treated alloy was found to be homogeneous throughout the specimen and approximately equal to the main composition, ~6wt% Al and ~4wt% V. Morphologically, martensite plates were formed from grain boundaries of the pre-existing β grains in an order, and no equilibrium α and β phase formations were detected in the microstructure. During aging of the martensitic structure, a variation in the size of the martensite plates and the concentration of the alloying elements were observed after 700 $^{o}$C. The microstructure obtained at 500 $^{o}$C, in Figure 5.1(d), seemed to be similar to WQ visually. Although the image characteristic of the martensite exhibited qualitative variations at 600 and 700 $^{o}$C, as in the images in Figure 5.1(e) and (f), there may be artifacts which might not reveal the underneath microstructural features. Also, the compositional analysis did not give any appreciable changes. The noticeable variation in the morphology of the martensite plate started in the specimen which was aged at 800 $^{o}$C as shown in Figure 5.1(g). The increase in the thickness of the martensite plate and the alloying element vanadium distribution could be descriptive. In Figure 5.1(h), where the martensite microstructure aged at 900 $^{o}$C, the amounts of alloying elements in the white regions (β phase) were detected as ~7.5wt% V and ~5.5wt% Al, and for dark regions (α phase) ~2.7wt% V and ~6.5wt% Al in this heat treatment.

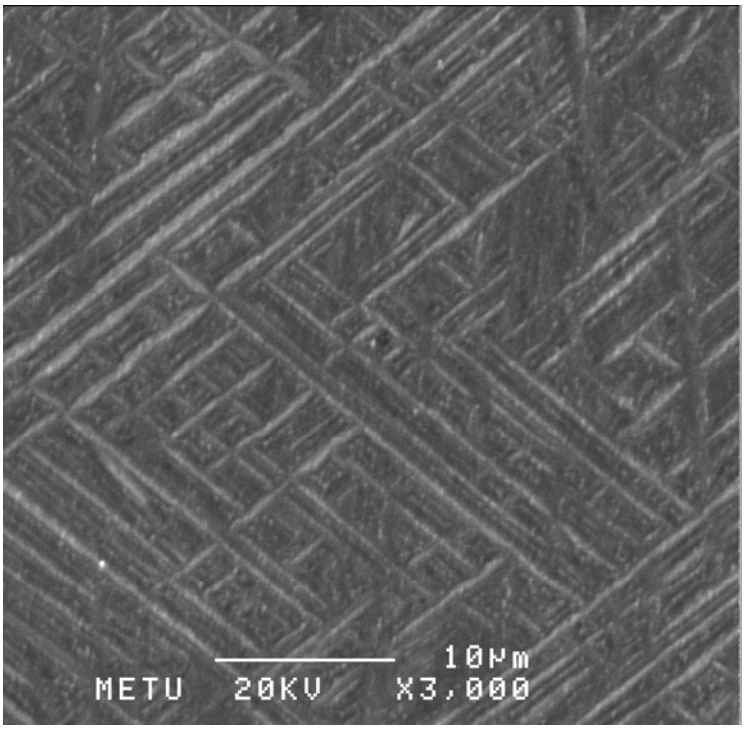



**(a)** FC

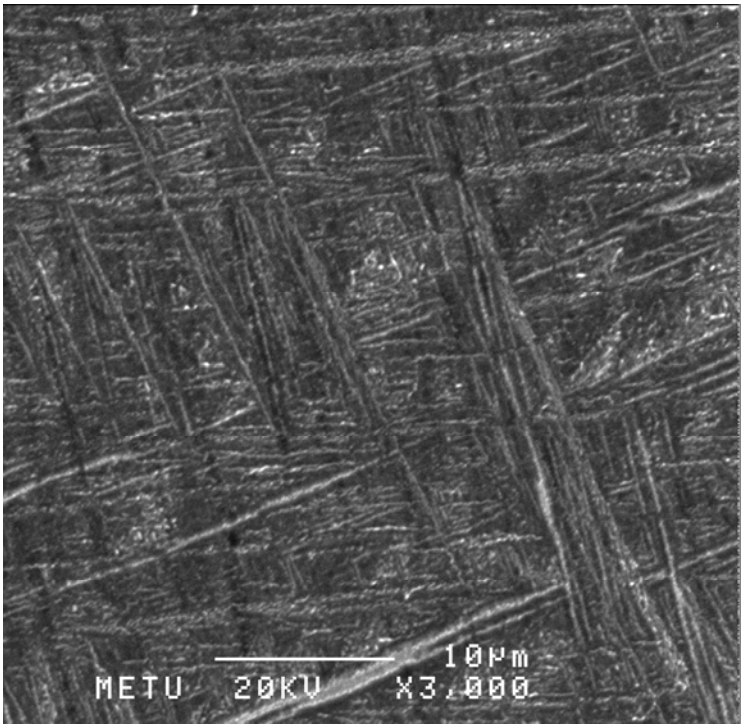



**(b)** AC

**Figure 5.1** SEM image of Ti-6Al-4V ELI alloy after heat treatments; **(a)** Furnace Cooled (FC), **(b)** Air Cooled (AC), **(c)** Water Quenched (WQ), WQ + Aged at **(d)** 500 $^{o}$C, **(e)** 600 $^{o}$C, **(f)** 700 $^{o}$C, **(g)** 800 $^{o}$C, **(h)** 900 $^{o}$C.

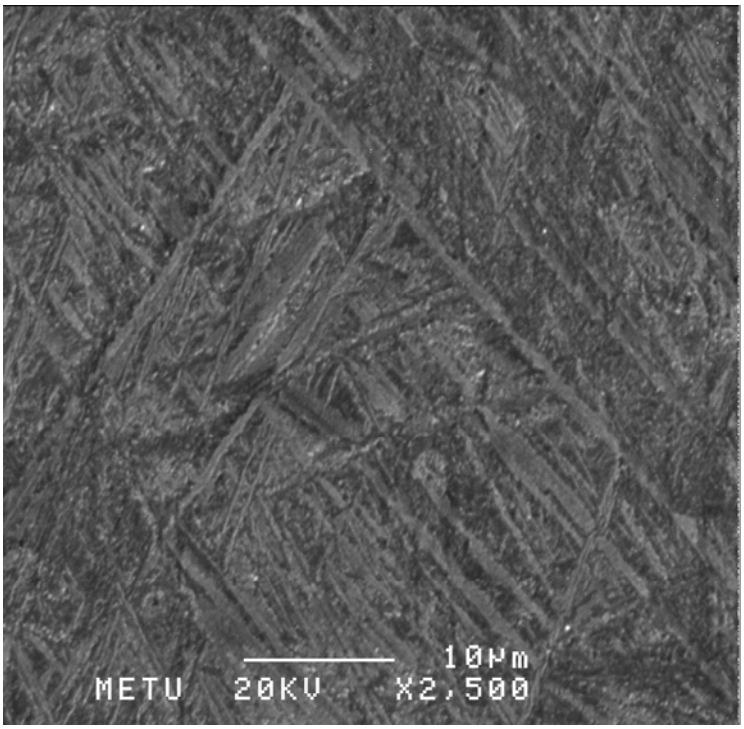



**(c)** WQ

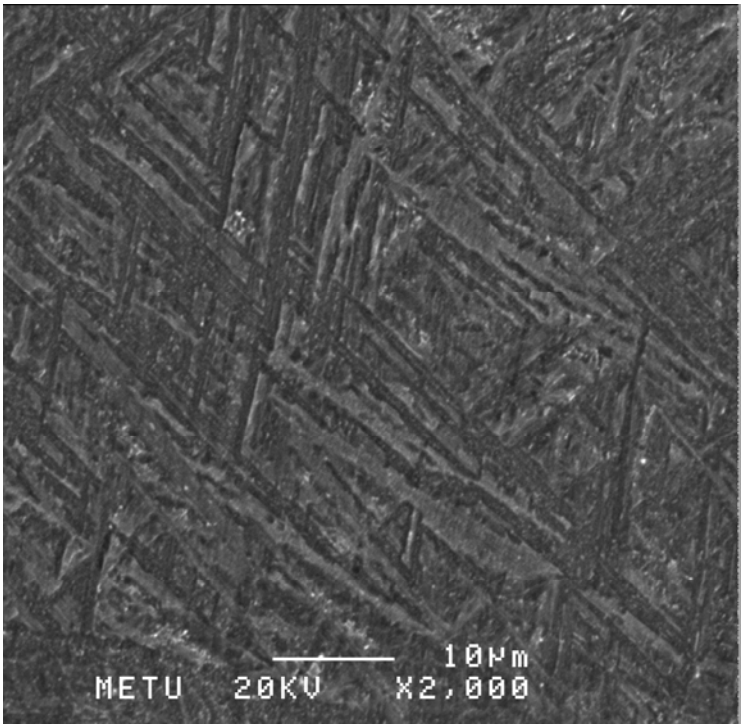



**(d)** WQ + 500

**Figure 5.1** (Continued)

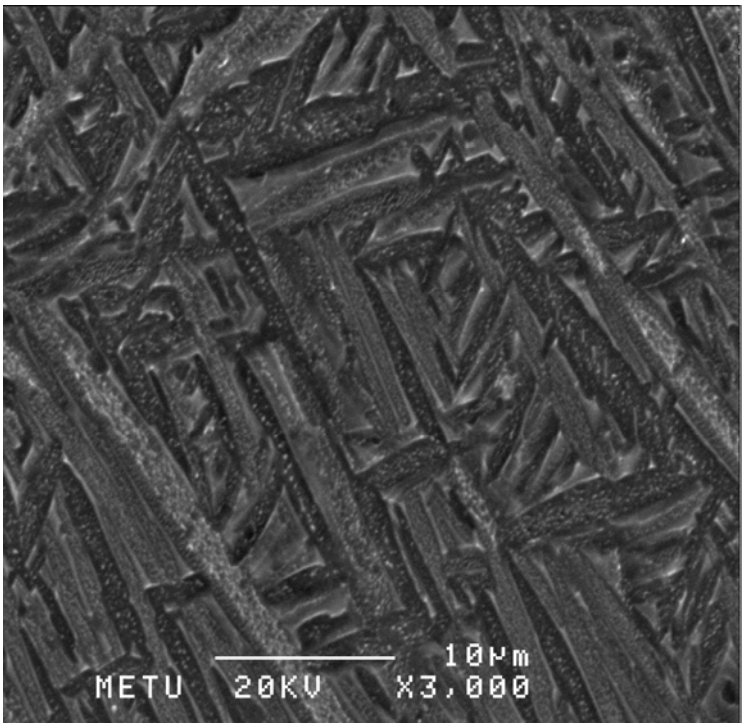



**(e)** WQ + 600

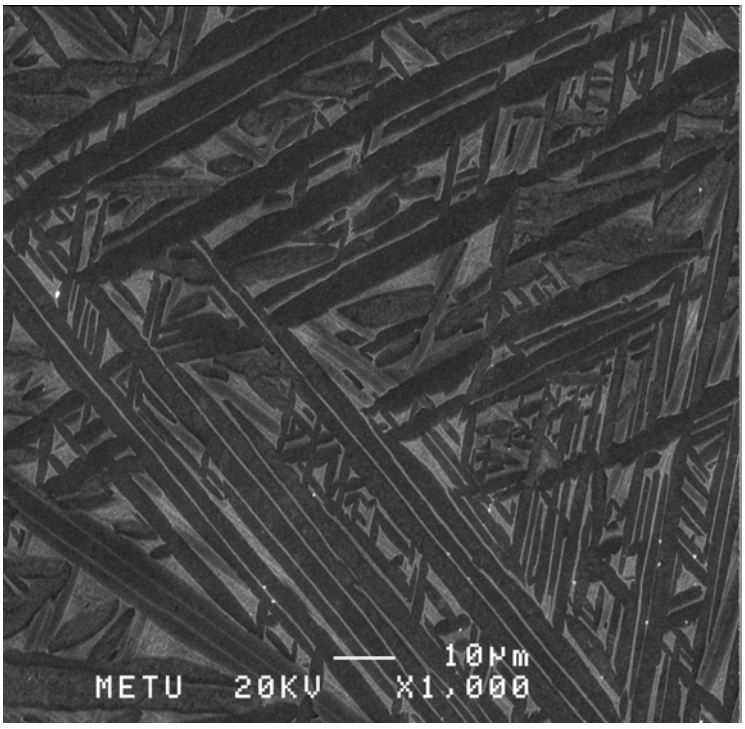



**(f)** WQ + 700

**Figure 5.1** (Continued)




**(g)** WQ + 800




**(h)** WQ + 900

**Figure 5.1** (Continued)

### 5.2 X – Ray Diffraction Analysis

The X – Ray Diffraction analysis were performed in order to detect the phase evolutions formed in the Ti-6Al-4V ELI alloy during heat treatments. According to the X – Ray Diffraction data, the 2θ and intensity (cps) values were obtained for every heat treatment and the lattice parameters; "c", "a", "c/a" and "unit cell volume" were calculated. The indices of the peaks of pure α and pure β, were given in Figure 5.2 and in Table 5.1. The experimental X – Ray diffractograms were given in Figure 5.3.

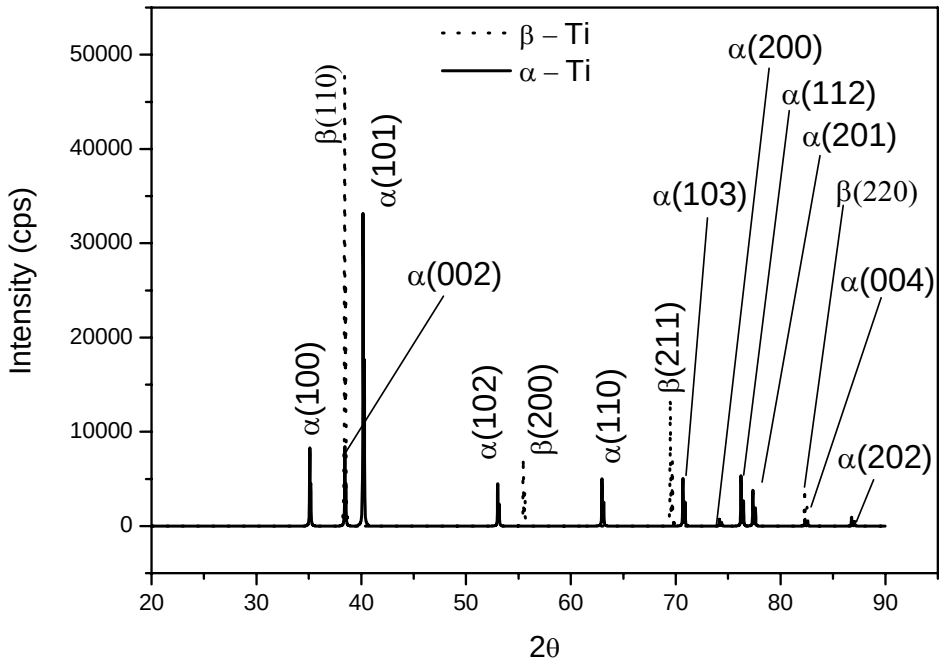



**Figure 5.2** The X – Ray diffraction pattern of pure α and pure β titanium.

**Table 5.1** The peak indices and diffraction angles of pure α and pure β titanium for Cu – $K_\alpha$. The lattice parameters of pure α - Titanium are 2.9503 Å for "a" and 4.681 Å for "c" values and "c/a ratio" is 1.5866. For pure β - Titanium, "a" value is 3.3112 Å [56].

| Pure α | |
|---|---|
| ***hkl*** | **2θ** |
| (100) | 35.093 |
| (002) | 38.430 |
| (101) | 40.177 |
| (102) | 53.017 |
| (110) | 62.958 |
| (103) | 70.684 |
| (200) | 74.165 |
| (112) | 76.231 |
| (201) | 77.367 |
| (004) | 82.331 |
| (202) | 86.777 |

| Pure β | |
|---|---|
| ***hkl*** | **2θ** |
| (110) | 38.416 |
| (200) | 55.455 |
| (211) | 69.478 |
| (220) | 82.293 |

The measured diffraction patterns of the specimens were given in Figure 5.3. In addition, the diffraction angles of the peaks were given in Table 5.2 below. The observed diffraction peaks were matched with α (spg 194) and with β (spg 229) crystal structures. It is found that, except for one peak, all peaks were due to the hexagonal α structure. That one peak which was around $39.5^o$ can be due to (110) diffraction in β, however, its presence even in WQ specimen made this conclusion questionable, whereas the peak in FC specimen at $39.863^o$ should be because of the presence of the β phase.

It is expected that for the specimen, which is cooled in furnace, the observed peaks should belong to the equilibrium α and β phases and for water quenched (WQ) specimen, peaks should belong to α'–martensite. In addition, an unknown peak was also observed in WQ specimen but the data to define this peak was not enough. It was thought that it might be due to a hydride or a nitride compound.

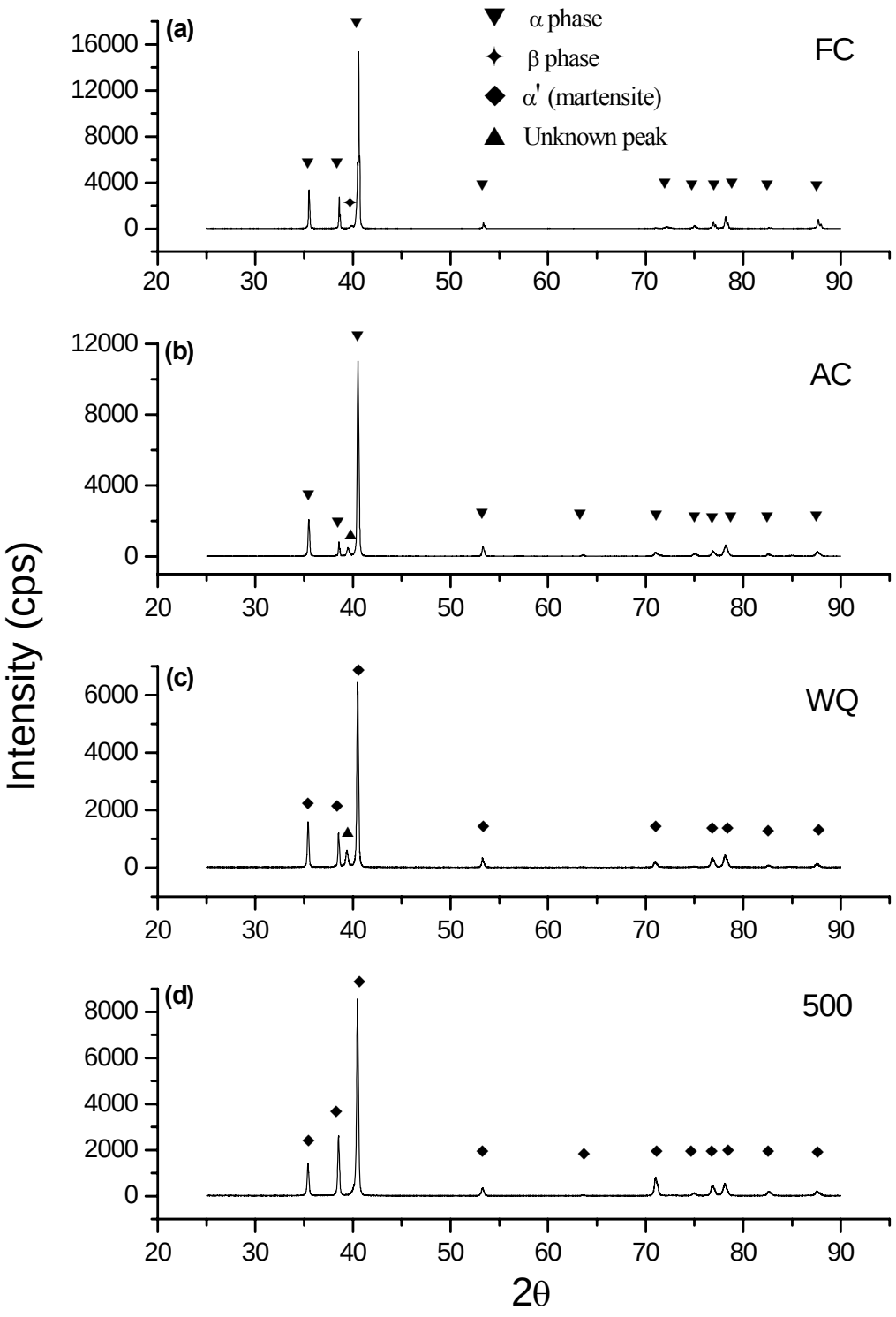



**Figure 5.3** The X-Ray Diffraction Patterns of all heat treated specimens; **(a)** Furnace Cooled (FC), **(b)** Air Cooled (AC), **(c)** Water Quenched (WQ), WQ + Aged at **(d)** 500 $^{o}$C for 10 hrs.

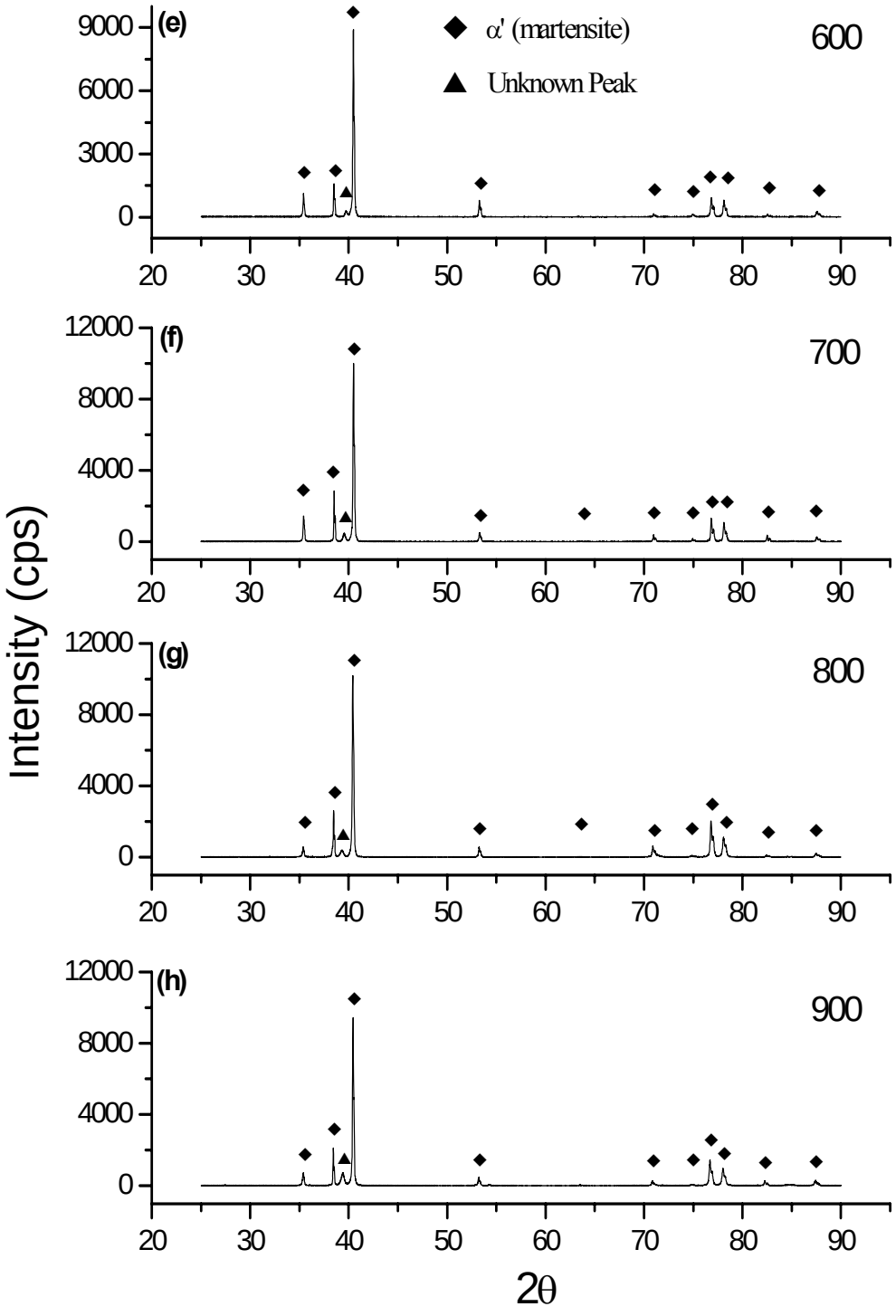



**Figure 5.3** (Continued) – The X-Ray Diffraction Patterns of aged specimens at (e) 600 $^{o}$C, (f) 700 $^{o}$C, (g) 800 $^{o}$C, (h) 900 $^{o}$C for 10 hrs.

The data obtained from X – Ray diffraction analysis was also used for evaluating the experimental lattice parameters; “a”, “c” and “c/a ratio” and unit cell volume which were given in Table 5.3 and in Figure 5.3. During calculations, firstly, (004) peak was used to evaluate “c” value for HCP crsytal structure. Secondly, in order to find the “a” value, (202) peak was used in Bragg’s Law and interplanar spacing formula of HCP, equations (4.1) and (4.2), respectively. Additionally, by using “c” and “a” values, unit cell volume was calculated for all heat treatment conditions to examine whether volume expansion occurred or not.

The investigation of diffraction angles of pure α-Ti and furnace cooled specimen exhibited that diffraction angles were shifted towards larger 2θ angles for all peaks due to the lattice parameter difference as can be seen in Table 5.1 – 5.3. Both “c” and “a” values for FC, AC and WQ were smaller than the pure state condition and inversly “c/a ratio” was higher. Among FC, AC and WQ specimens, the smallest “c” and “a” values belonged to FC specimen. The AC specimen showed largest “c” value and for “a” value the WQ specimen had the largest.

**Table 5.2** The diffraction angles and the indices of the peaks for all heat treated specimens

| hkl / Heat Treatment | (100) | (002) | Unknown Peak | (101) | (102) | (110) | (103) | (200) | (112) | (201) | (004) | (202) |
|---|---|---|---|---|---|---|---|---|---|---|---|---|
| **FC** | 35.488 | 38.598 | 39.863 | 40.592 | 53.366 | -- | 71.028 | 74.973 | 76.918 | 78.198 | 82.618 | 87.663 |
| **AC** | 35.474 | 38.558 | 39.487 | 40.515 | 53.324 | 63.526 | 70.962 | 75.027 | 76.886 | 78.181 | 82.529 | 87.604 |
| **WQ** | 35.406 | 38.526 | 39.390 | 40.478 | 53.257 | -- | 70.971 | 74.883 | 76.817 | 78.117 | 82.583 | 87.517 |
| **500** | 35.386 | 38.528 | -- | 40.464 | 53.267 | 63.525 | 71.022 | 74.976 | 76.847 | 78.099 | 82.574 | 87.554 |
| **600** | 35.418 | 38.501 | 39.728 | 40.473 | 53.249 | -- | 70.936 | 74.948 | 76.826 | 78.101 | 82.527 | 87.537 |
| **700** | 35.419 | 38.517 | 39.539 | 40.490 | 53.271 | 63.573 | 70.933 | 74.906 | 76.814 | 78.124 | 82.482 | 87.534 |
| **800** | 35.380 | 38.475 | 39.323 | 40.420 | 53.237 | 63.429 | 70.886 | 74.878 | 76.805 | 78.071 | 82.423 | 87.466 |
| **900** | 35.387 | 38.442 | 39.392 | 40.439 | 53.209 | -- | 70.837 | 74.848 | 76.692 | 78.013 | 82.271 | 87.400 |

**Table 5.3** Lattice parameters for the hexagonal α or α' phases and unit cell volume for all heat treated specimens and pure α-Ti. (*) was for experimental value of "a" and "c" for FC and WQ in Malinov et. al. study [9].

| Heat Treatment | a | c | c/a | Unit Cell Volume |
|---|---|---|---|---|
| **FC** | 2.9219 | 4.6676 | 1.5975 | 103.531 |
| **FC (exp)*** | 2.938 | 4.668 | 1.5888 | 104.685 |
| **AC** | 2.9231 | 4.6717 | 1.5982 | 103.713 |
| **WQ** | 2.9266 | 4.6693 | 1.5954 | 103.904 |
| **WQ (exp)*** | 2.935 | 4.668 | 1.5905 | 104.472 |
| **500** | 2.9253 | 4.6697 | 1.5963 | 103.817 |
| **600** | 2.9255 | 4.6718 | 1.5969 | 103.879 |
| **700** | 2.9252 | 4.6739 | 1.5978 | 103.905 |
| **800** | 2.9270 | 4.6767 | 1.5978 | 104.097 |
| **900** | 2.9280 | 4.6838 | 1.5997 | 104.326 |
| **Pure α-Ti** | 2.9503 | 4.681 | 1.5866 | 105.858 |

The variations in lattice parameters were also seen in the aged conditions. Although the increase in "a" value was seen after 700 $^{o}$C, the "c" value increased continuously from WQ to WQ + Aged at 900 $^{o}$C which caused an increase in "c/a ratio". For the unit cell volume point of view, an increase can easily be seen in Figure 5.4(d) from FC to WQ and same increasing characteristic can be said for WQ and aged specimens. The expansion of the unit cell for aged martensite might be due to the vanadium element release from the martensite phase. According to the metalic radius, which was 1.47 Å for titanium element and 1.36 Å for vanadium element, the replacement of vanadium atoms with titanium atoms may cause a volumetric expansion in the unit cell. The lattice expansion of the α phase was explained by Elmer et. al. [57] due to V element diffusion during heating from room temperature. They observed that between 550 and 750 $^{o}$C, the expansion rate of the α phase decreased and the V content of the α phase became maximum at 700 $^{o}$C which resulted a decrease in the lattice parameter of the α phase. After 700 $^{o}$C, an increase was observed in the lattice parameter and the unit cell volume.

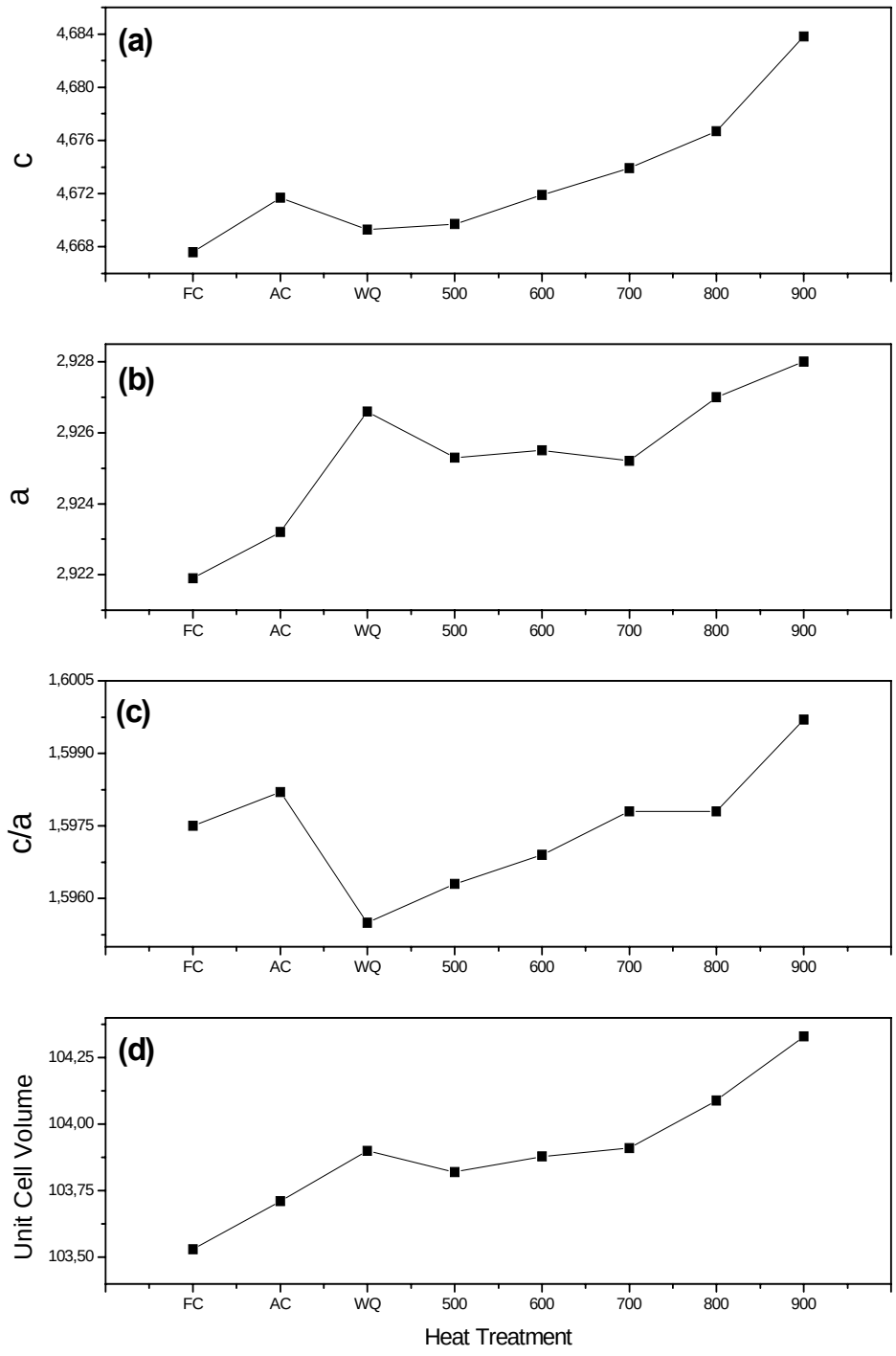



**Figure 5.4** The lattice parameters; **(a)** c, **(b)** a , **(c)** c/a ratio, and **(d)** unit cell volume for all heat treated specimen

The investigations about variation in the lattice parameters and the unit cell volume showed that the martensite structure of Ti-6Al-4V ELI alloy system, interestingly did not exhibit a shift towards equilibrium α phase during aging procedure.

### 5.3 Hardness Measurements

In order to define the microstructural variations in Ti-6Al-4V ELI alloy system, hardness measurements were also made as shown in Figure 5.5. The minimum hardness values were obtained from furnace cooled specimen which had equilibrium α and β phases. Hardness increases for air cooled specimen and WQ and WQ + Aged specimens. It is obvious that aging of martensite has higher hardness values than as quenched form. Although the hardness values of aged specimens exhibited a parabolic distribution, the margin of error may alleviate this.

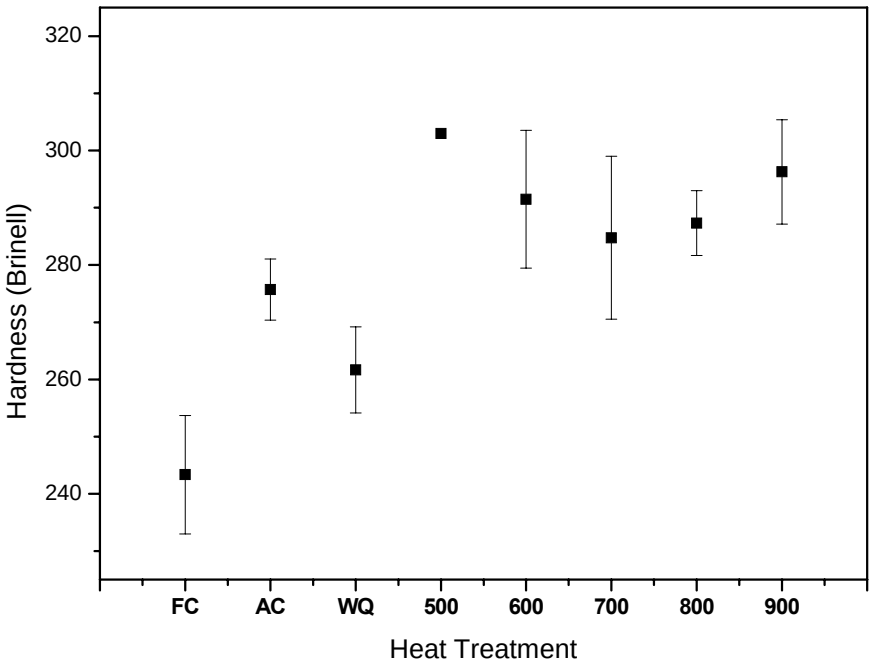



**Figure 5.5** Hardness values of all heat treated specimens.

### 5.4 Corrosion Measurements

The corrosion measurements can be divided into two as open circuit potential (OCP) measurements and anodic polarization measurements which include also computational corrosion rate calculations.

#### 5.4.1 Open Circuit Potential (OCP) Measurements

The measurements were done in Ringer's solution for four days and data was recorded in equal time intervals. As shown in Figure 5.6, long time immersions in Ringer's solution at 37 $^{o}$C exhibited passive film formation on the surface of the specimens which shifted the OCP values to nobler values.

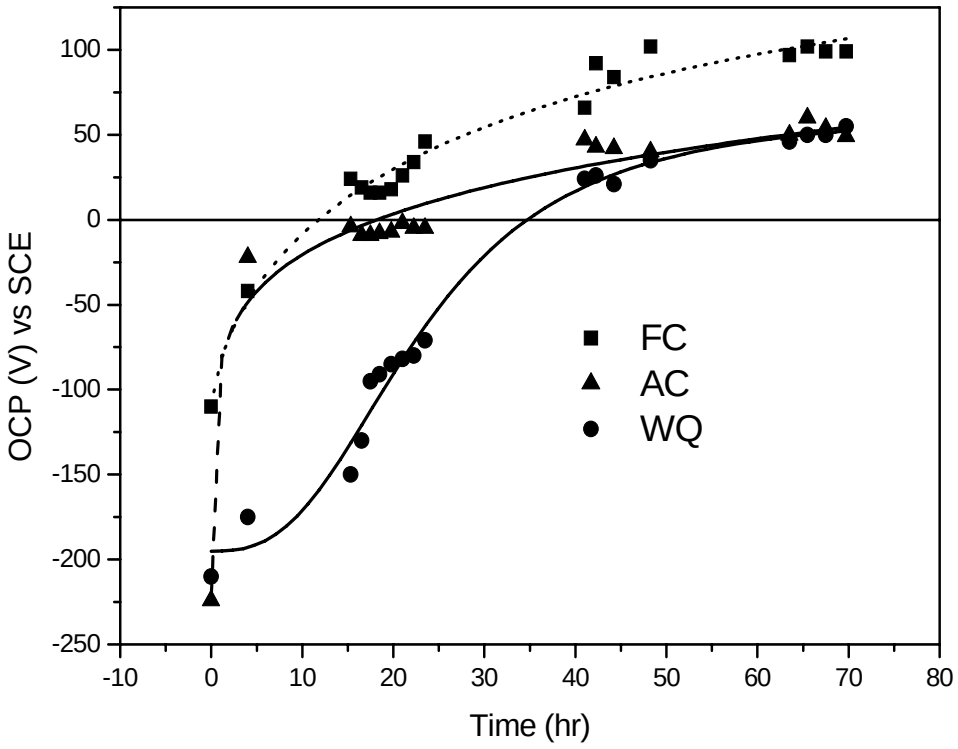



**Figure 5.6** The OCP data for all heat treated specimens in Ringer's solution at 37 $^{o}$C.

The increase in the OCP values showed that within the first 5 hours period, the rate of passive film formation had the highest value, and after 40 hours, the rate of increase became much less with respect to the early stages of film formation. The specimens, which were furnace cooled and WQ + Aged at 800 $^{o}$C for 10 hours, had the highest OCP values. Air cooled and as quenched ones had also more noble OCP values than the aged ones. But as a general point of view, all the potentials started from (-250 mV) shift to nobler values. The same behavior was seen in the OCP values of the experiment, which was done in 0.2M NaF added Ringer's solution, but because of $F^-$ ion effect in the solution, OCP values did not increase up to the values as in Ringer's solution without NaF and the starting potentials decreased to a range of (-400) to (-500) mV. Again within first 5 hours period the rate of passive film formation was very high but they reached the maximum values after 1 day immersion period. Also because of the aggressive behavior of $F^-$ ions in the solution, the starting potentials of the OCP measurements were all lowered with respect to the solution without NaF.

### 5.4.2 Activation Polarization

The aim of activation polarization measurements was to characterize the corrosion behavior of the heat treated specimens according to the microstructural developments and evaluating corrosion rates in Ringer's solution and 0.1M and 0.2M NaF added Ringer's solutions at 37 $^{o}$C. Two different surface treatments, which were passive filmed formed surface by long term immersion in Ringer's solution at 37 $^{o}$C and the other as polished, were tested in three different corrosion mediums as Ringer's solution without NaF, 0.1M and 0.2M NaF added Ringer's solutions. The obtained data was then input to a computer program to calculate the corrosion potentials, current densities and corrosion rates. The given Figures 5.7 – 5.10 below showed variations with respect to potential and current densities in the order of passive film formed surfaces in Ringer's solution, as polished surfaces in Ringer's solution, as polished surfaces in 0.1M and 0.2M NaF added Ringer's solution.

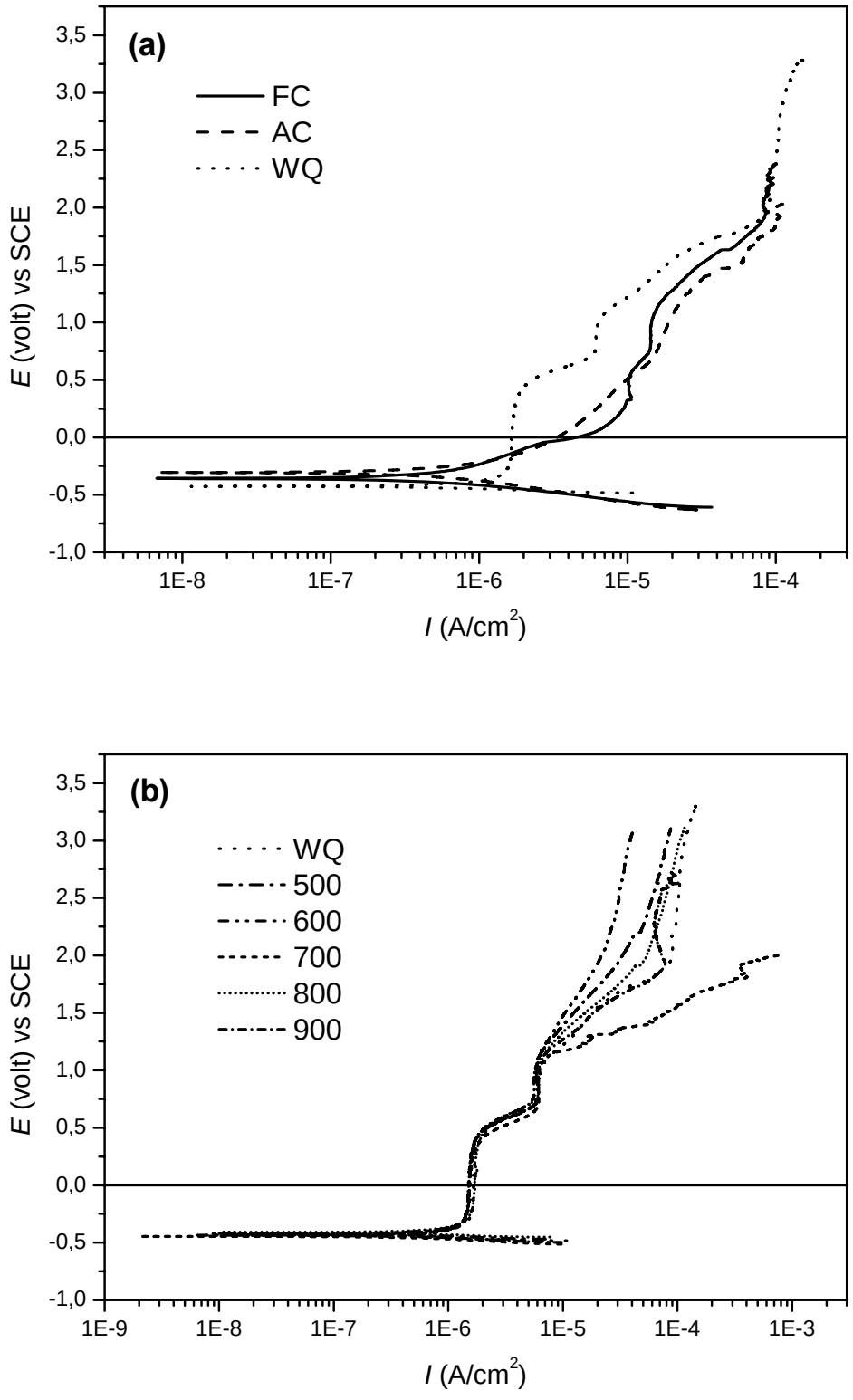



**Figure 5.7** *E* vs *I* graph for **(a)** FC, AC and WQ specimens and **(b)** WQ, WQ + Aged at 500, 600, 700, 800, 900 $^{o}$C for 10 hrs specimens which had passive films on their surfaces in Ringer's solution.

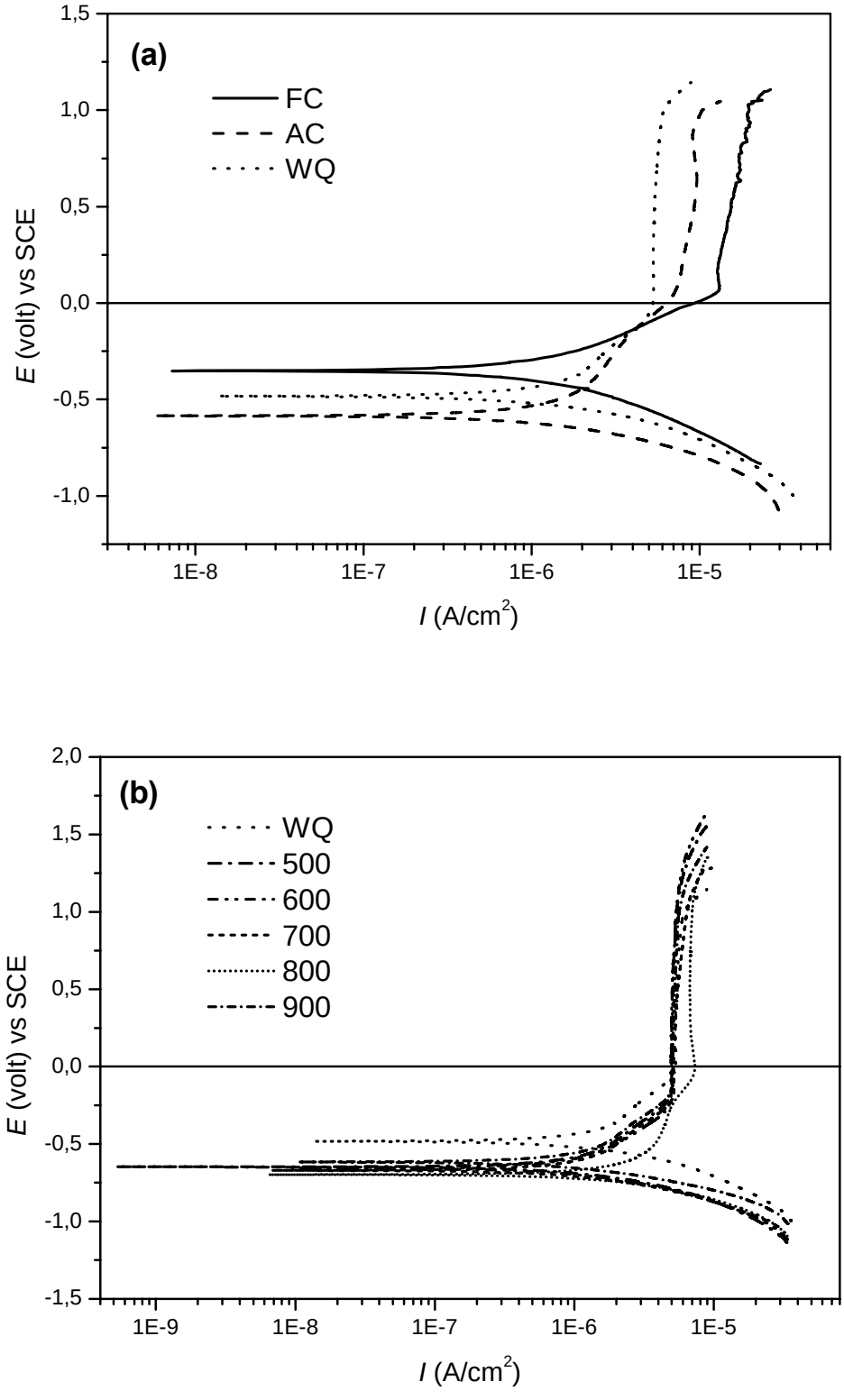



**Figure 5.8** *E* vs *I* graph for **(a)** FC, AC and WQ specimens and **(b)** WQ, WQ + Aged at 500, 600, 700, 800, 900 $^{o}$C for 10 hrs specimens for as polished surface condition in Ringer's solution.

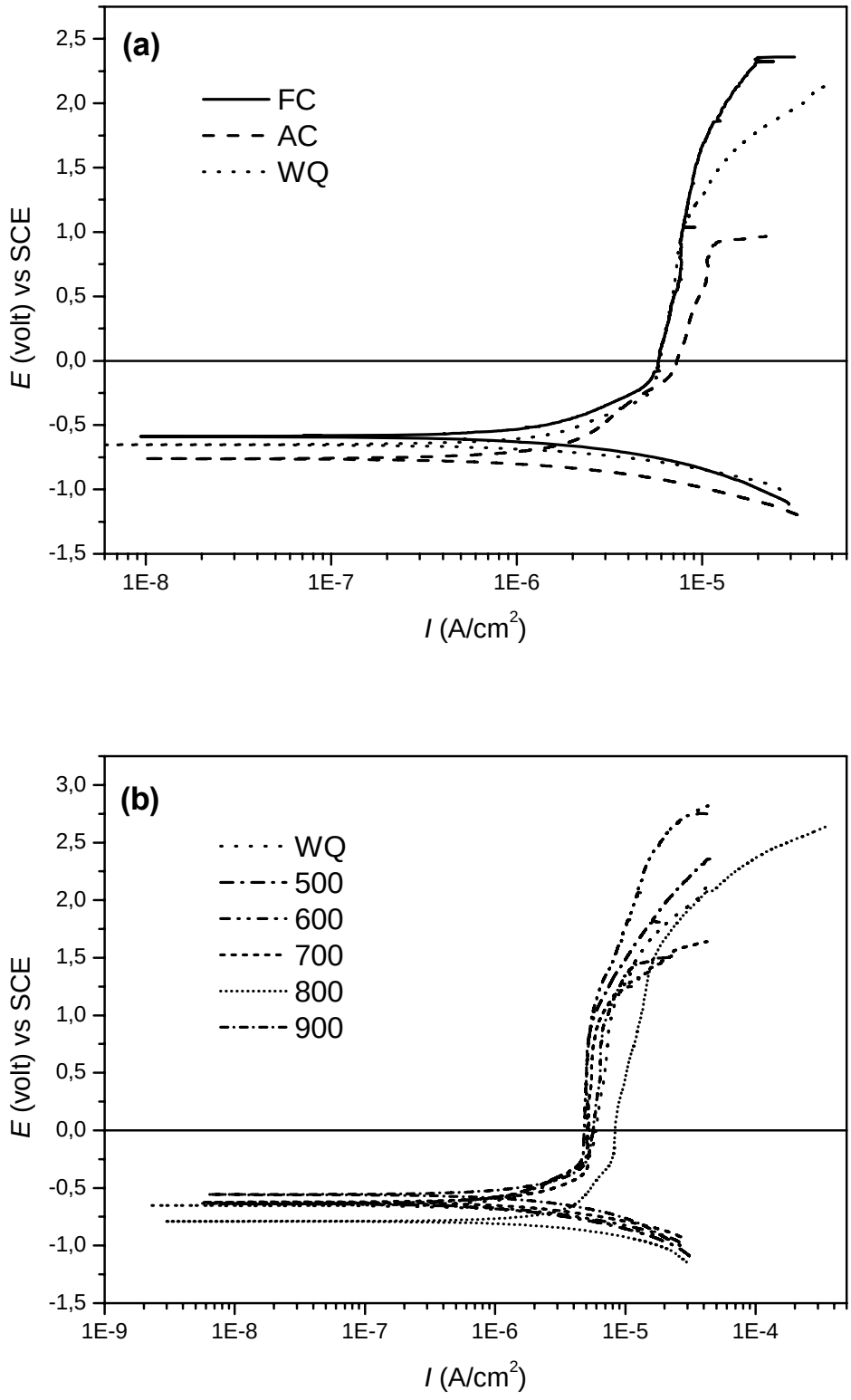
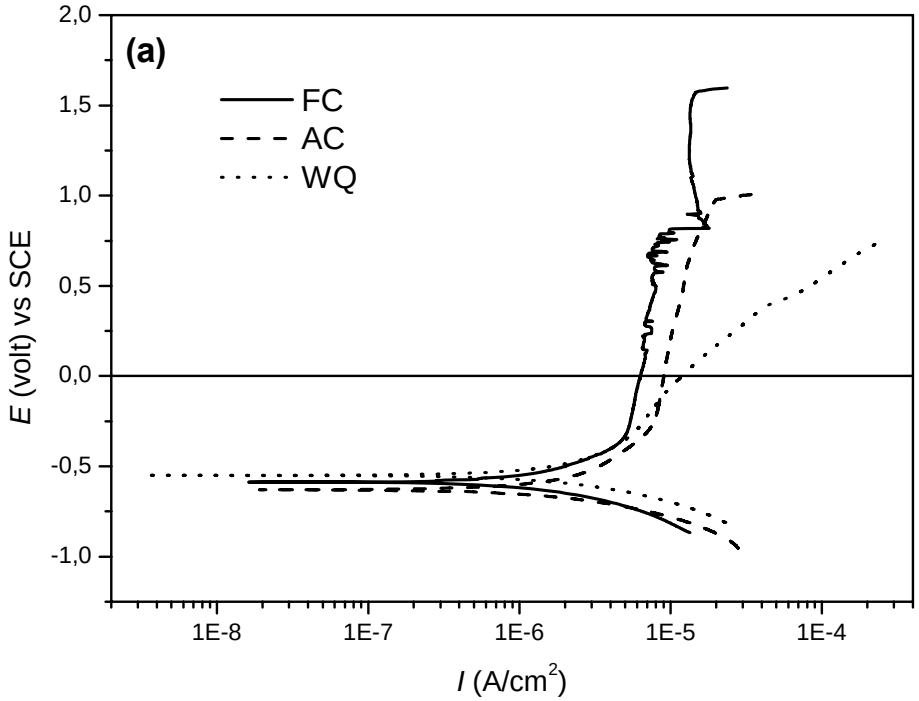



**Figure 5.9** *E* vs *I* graph for **(a)** FC, AC and WQ specimens and **(b)** WQ, WQ + Aged at 500, 600, 700, 800, 900 $^{o}$C for 10 hrs specimens for as polished surface condition in 0,1M NaF added Ringer's solution.



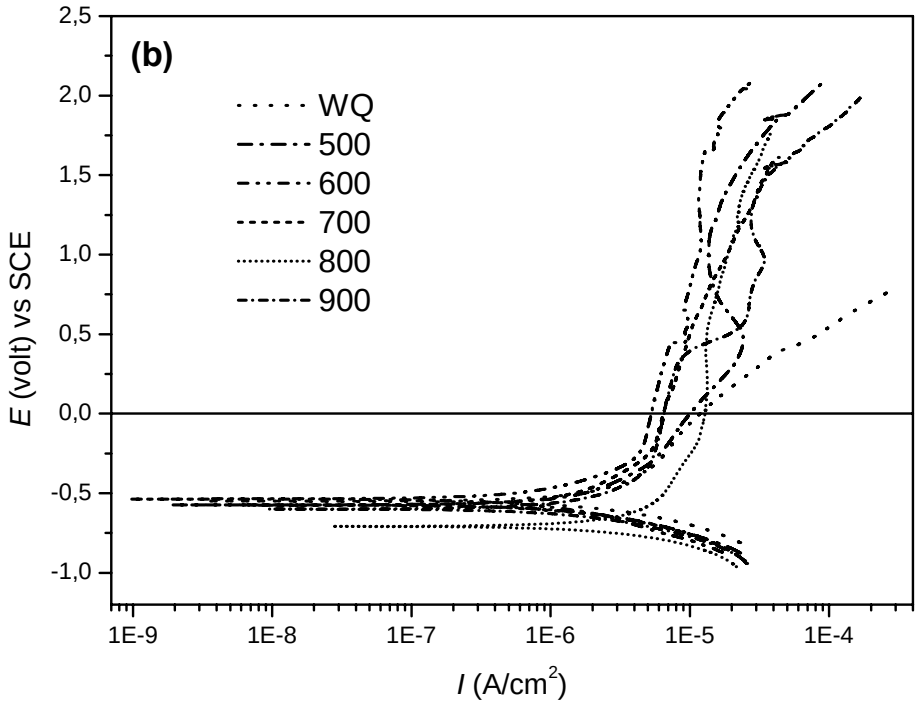




**Figure 5.10** *E* vs *I* graph for **(a)** FC, AC and WQ specimens and **(b)** WQ, WQ + Aged at 500, 600, 700, 800, 900 $^{o}$C for 10 hrs specimens for as polished surface condition in 0,2M NaF added Ringer's solution.

The computational corrosion potentials, current densities and corrosion rates and passivation potential, $E_{pas}$, and passivation current, $I_{pas}$, data were given in the Table 5.4 and Table 5.5, respectively.

**Table 5.4** The computational results of $E_{corr}$, $I_{corr}$, $R_p$, $B$, and corrosion rate, $r$, for all specimens with respect to all surface and corrosion medium conditions.

| Surface & Medium Condition | Heat Treatment | $E_{corr}$ (mV) | $I_{corr}$ (A/cm$^2$) (x10$^{-7}$) | $R_p$ (Ω cm$^2$) | $B$ | $r$ (mm/year) |
|---|---|---|---|---|---|---|
| Passive Film Formed Surface in Ringer's Soln. with no NaF | FC | -358.23 | 2.5864 | 83027 | 0.02147 | 0.00225 |
| | AC | -305.25 | 2.1510 | 83601 | 0.01798 | 0.00187 |
| | WQ | -426.11 | 7.5764 | 26819 | 0.02032 | 0.00658 |
| | 500 | -422.34 | 7.7929 | 28769 | 0.02242 | 0.00677 |
| | 600 | -436.75 | 7.0092 | 28708 | 0.02012 | 0.00609 |
| | 700 | -445.77 | 8.5489 | 32248 | 0.02757 | 0.00742 |
| | 800 | -411.68 | 7.0621 | 26836 | 0.01895 | 0.00613 |
| | 900 | -432.23 | 11.825 | 32490 | 0.03842 | 0.01027 |
| As polished surface in Ringer's Soln. with no NaF | FC | -351.49 | 7.1745 | 53751 | 0.03856 | 0.00623 |
| | AC | -584.99 | 9.3447 | 43668 | 0.04081 | 0.00811 |
| | WQ | -482.42 | 8.5055 | 40595 | 0.03453 | 0.00738 |
| | 500 | -647.26 | 3.1430 | 49680 | 0.01561 | 0.00273 |
| | 600 | -656.03 | 3.6310 | 49339 | 0.01792 | 0.00315 |
| | 700 | -669.72 | 7.0179 | 45825 | 0.03216 | 0.00609 |
| | 800 | -697.64 | 12.245 | 26472 | 0.03241 | 0.01063 |
| | 900 | -615.44 | 4.1556 | 46654 | 0.01939 | 0.00361 |
| As polished surface in 0.1M NaF added Ringer's Soln | FC | -589.27 | 2.5267 | 53226 | 0.01349 | 0.00219 |
| | AC | -761.35 | 3.3782 | 45345 | 0.01532 | 0.00293 |
| | WQ | -652.64 | 10.631 | 37944 | 0.04034 | 0.00923 |
| | 500 | -637.8 | 6.7850 | 49418 | 0.03353 | 0.00589 |
| | 600 | -635.14 | 8.2110 | 43298 | 0.03555 | 0.00713 |
| | 700 | -622.28 | 9.8674 | 32006 | 0.03158 | 0.00857 |
| | 800 | -789.99 | 19.256 | 21489 | 0.04138 | 0.01672 |
| | 900 | -557.44 | 11.310 | 33782 | 0.03821 | 0.00982 |
| As polished surface in 0.2M NaF added Ringer's Soln | FC | -586.57 | 8.6029 | 25587 | 0.02201 | 0.00747 |
| | AC | -629.72 | 11.902 | 26038 | 0.03099 | 0.01033 |
| | WQ | -549.86 | 15.088 | 25258 | 0.03811 | 0.0131 |
| | 500 | -573.71 | 10.901 | 33131 | 0.03612 | 0.00946 |
| | 600 | -535.52 | 2.4459 | 61385 | 0.01501 | 0.00212 |
| | 700 | -574.03 | 8.4950 | 37393 | 0.03177 | 0.00738 |
| | 800 | -708.55 | 22.358 | 16509 | 0.03691 | 0.01941 |
| | 900 | -599.68 | 10.585 | 32059 | 0.03393 | 0.00919 |

**Table 5.5** The passivation potentials, $E_{pas}$ and passivation current densities, $I_{pas}$, of all heat treated specimens.

| Heat Treatment/ Surface & Medium | Passive Film Formed Surface in Ringer's Soln. with no NaF | | As polished surface in Ringer's Soln. with no NaF | | As polished surface in 0.1M NaF added Ringer's Soln | | As polished surface in 0.2M NaF added Ringer's Soln | |
|---|---|---|---|---|---|---|---|---|
| | $E_{pas}$ (mV) | $I_{pas}$ (A/cm$^2$) (x10$^{-6}$) | $E_{pas}$ (mV) | $I_{pas}$ (A/cm$^2$) (x10$^{-6}$) | $E_{pas}$ (mV) | $I_{pas}$ (A/cm$^2$) (x10$^{-6}$) | $E_{pas}$ (mV) | $I_{pas}$ (A/cm$^2$) (x10$^{-6}$) |
| **FC** | 152 | 8.04 | 69 | 13.1 | -153 | 5.62 | -298 | 5.21 |
| **AC** | - | - | 96 | 7.44 | -93 | 6.89 | -226 | 7.98 |
| **WQ** | -258 | 1.58 | 2 | 5.28 | -175 | 5.54 | - | - |
| **500** | -276 | 1.41 | -176 | 4.92 | -219 | 4.72 | 451 | 24.1 |
| **600** | -272 | 1.43 | -203 | 4.91 | -194 | 5.06 | 1047 | 12.0 |
| **700** | -300 | 1.41 | -171 | 5.17 | -311 | 5.13 | - | - |
| **800** | -242 | 1.49 | -20 | 7.30 | -190 | 8.13 | 76 | 13.1 |
| **900** | -289 | 1.38 | -130 | 5.04 | -213 | 5.20 | - | - |

As shown in Figure 5.7(a) and (b), anodic polarization diagrams exhibited different corrosion behavior according to the heat treatment applied. The initial potentials to the experiments were from 0.5 V below $E_{corr}$ to 3.5 V vs SCE. It was pointed out that the corrosion potentials in OCP measurements in Figure 5.6 seemed not to be equal to the anodic polarization corrosion potentials. This was because of some film dissolution at the cathodic potentials at the beginning of the experiment. When the corrosion potentials, $E_{corr}$, were examined, it was obvious that for the furnace cooled specimen, $E_{corr}$ value was more noble than for as quenched and all aged specimens. Since the equilibrium phases in Ti-6Al-4V ELI alloy system exhibited uneven distribution of alloying elements of aluminum and vanadium under slow cooling conditions, in FC specimen there seems to be a more protective. Geetha et. al. [51] explained this relation as the distribution of alloying elements present in various phases. But also it was reported that V and Al did not form separate phases within the film, they were present as cations in substitutional or interstitial sites [3]. The vanadium content at the surface

decreased with respect to the bulk, indicating no preferential diffusion of vanadium element towards the surface. On the other hand, the aluminum content strongly increased from bulk to surface, showing a clear diffusion of the aluminum element towards surface of the material to form passive layer [3]. The alloying elements Al and V were present throughout the film in their most stable oxidation states as $Al_2O_3$ and $V_2O_5$, respectively [3]. Aluminum is reported to be present throughout the oxide film, but with a tendency to be more strongly enriched at the outermost surface (i.e. at the oxide/air or oxide/liquid interface) [58], inversly, vanadium seems to be present closer to the oxide/metal interface rather than uniformly distributed across the oxide layer thickness [59]. According to that the composition of the passive film formed on the surface of FC specimen had higher $Al_2O_3$ content than the oxide of vanadium, where mostly $Al_2O_3$ placed on the surface of the α phase and oxide of vanadium on the β phase [3]. But aluminum enrichment and/or vanadium depletion of the α phase resulted in preferential dissolution of the α phase during anodic polarization at higher potentials as shown in Figure 5.7(a). On the other hand, WQ specimen, which is α'-martensite, exhibited lower passive current density value, $I_{pas}$, than FC and AC specimens as given in Table 5.5. This structure consists of all the alloying elements within itself and no partitioning has occurred on this treatment where a homogeneous distribution of alloying elements had taken place. A homogeneous V content of the underlying martensitic microstructure resulted in a higher V content in the passive film all throughout the surface of the material. In addition, the stability of the passive film of the AC specimen was not good enough with respect to FC and WQ specimens, WQ being more stable, which can easily be seen in Figure 5.7(a). For AC specimen, it was obvious that a passive film formation was seen at OCP conditions but on the other hand, the dissolution of the passive film during anodic polarization was also observed where the current density increased continuously as shown in Figure 5.7(a) and Table 5.5. The passive film formation and its stability exhibited very characteristic behavior for as quenched and all aged specimens showing two step passivations. As given in Table 5.5, the passivation potentials and current densities varied -240 to -300 mV and $(1.4 – 1.5)x10^{-6}$ A/cm$^2$ for aged specimens. The step behavior is because of

the existence of a previously formed passive film and it has stable character during anodic polarization. The repassivation at higher potentials could easily be seen in Figures 5.7(a) and (b). In WQ and WQ + Aged specimens, all the passive film breakdown potentials were at similar potentials around 1.1 V and $6x10^{-6}$ $A/cm^2$ and after this stage, the slope ($m$) of the $E$ vs $I$ diagram exhibited variations which were ordered as $m_{600} > m_{500} > m_{800} > m_{WQ} > m_{900} > m_{700}$.

The $E$ vs $I$ graphs of as polished surface treated specimens were given in Figure 5.8(a) and (b). The two step passivation characteristic of the WQ and aged specimens was not observed under polished surface condition which exhibited only one passive region. Among FC, AC and WQ specimens, the highest variation in $E_{corr}$ value was observed for AC, which shifted in active direction from -305 to -585 mV due to the absence of previously formed passive film on the surface. This increase was also seen in WQ specimen but not in FC. In other words, the basket-weave type of α microstructure with respect to the Widmanstätten α was more susceptible to corrosion according to the absence of the elemental distributions in the two phases of AC specimen as shown in Table 5.4. The behavior of AC specimen which had previously formed passive film on its surface exhibited that the passive film could not repair itself during anodic polarization as FC and WQ, but the dissolution of the passive film occurred. In as polished surface condition, AC specimen exhibited passivation up to 1.1 V with higher passive current densities. For the aged specimens point of view, the absence of the previously formed passive film caused a change in $E_{corr}$ from around -430 to around -670 mV. The variations in $I_{corr}$ was not much observable. Only WQ and WQ + Aged specimen at 800 $^{o}$C had higher $I_{corr}$ values than the previously passive film formed case. But the appreciable variation could be seen in FC and AC specimens in Table 5.4. The absence of previously formed passive film at the surface of FC and AC specimens increased corrosion rates although passivation was observed at higher current densities during anodic polarization. In addition, the potentials of passive film formation exhibited that while the potential increased in the noble direction for WQ and aged specimens, for FC it decreased.

The variations in passive current densities for WQ and aged specimens with respect to the previously passive film formed case were 2 times higher than FC as shown in Table 5.5. Among WQ and aged specimens, the specimen aged at 800 $^{o}$C exhibited the highest values for $I_{corr}$, $I_{pas}$ and nobler values for $E_{corr}$ and $E_{pas}$.

The dissolution of the passive film discussed above explained by Metikoš-Huković et. al. [46] as a release of Al and V metal ions into the environment. The passive film is a mixture of oxides, but a local corrosion might take place by means of anion penetration. For Ti-6Al-4V alloy system, V ion release produced a diffusion of vacancies in the oxide layer. Additionally, the presence of $Cl^-$ ions at high concentrations in the solution caused their absorption into the oxygen vacancies on the surface. The stability of oxide layer decreased and a possibility of a breakdown of the passive film was appeared.

Corrosion behavior of the heat treated specimens showed different characteristics due to the addition of NaF to the Ringer's solution which made the solution a more aggressive medium. In order to understand the $F^-$ ion effect, two different NaF concentrations were prepared. After addition of NaF, the $E$ vs $I$ graph exhibited limited passivation for almost all specimens for 0.1M NaF but a very difficult passivation was seen in 0.2M NaF added Ringer's solution which were shown in Figures 5.9(a) - (b) and 5.10(a) - (b).

The addition of 0.1M NaF exhibited an increase in the $E_{corr}$ values but a decrease in $I_{corr}$ values of FC and AC with respect to the specimens with as polished surface treatment in Ringer's solution with no NaF as shown in Figure 5.9(a) and Table 5.4. This increase was also seen in WQ specimen for $E_{corr}$ values from -482 to -653 mV and for $I_{corr}$ which changed from $8.5 \times 10^{-7}$ to $1.06 \times 10^{-6}$ A/cm$^2$. Among aged specimens, specimen aged at 800 $^{o}$C also exhibited an increase for $E_{corr}$ and $I_{corr}$ as WQ, but the others had lower $E_{corr}$ with respect to the as polished surface specimens in Ringer's solution with no NaF. The effect of NaF addition on the passivation potentials and current densities were

considerable. Although the $E_{pas}$ values of almost all specimens were increased in the active direction, the $I_{pas}$ values did not show appreciable variation except specimen aged at 800 $^{o}$C and FC. As given in Table 5.5, for FC $I_{pas}$ decreased to 5.62x10$^{-6}$ A/cm$^{2}$ and for aged specimen at 800 $^{o}$C it increased to 8.13x10$^{-6}$A/cm$^{2}$. Also the passive film breakdown potential decreased for AC to below 1V with the addition of NaF with respect to the as polished surface condition with no NaF as shown in Figure 5.8(a) and 5.9(a). Schmidt and Azambuja [60] explained the detrimental effect of fluoride ions on passivation behavior of Ti-6Al-4V as the adsorption of fluoride ions on the passive film, which caused its dissolution and/or the formation of a porous layer. Accordingly, the protectiveness of the oxide film decreased.

When the amount of NaF increased from 0.1M to 0.2M, the corrosion resistance behavior changed drastically as shown in Figures 5.10(a) and (b). The effect of $F^{-}$ ion during passivation could easily be determined from this experimental condition. Although an increase was observed for $E_{corr}$ values in the noble direction with respect to the 0.1M NaF added condition for FC, AC and WQ, the increase in the $I_{corr}$ was more appricable. The response of FC and AC specimens to the addition of 0.2M NaF was higher than WQ and WQ + Aged specimens for equilibrium corrosion conditions as shown in Table 5.4. But during anodic polarization, as shown in Figure 5.10(a) and (b), the reaction to the addition of 0.2M NaF was higher for WQ and WQ + Aged specimens. The behavior of $E$ vs $I$ graph is anodic active polarization behavior instead of an active to passive transition behavior. The aged specimens at 600 and 700 $^{o}$C had lower $I_{corr}$ values, 2.45x10$^{-7}$ and 8.5x10$^{-7}$ A/cm$^{2}$ respectively, than WQ and other aged specimens in 0.2M NaF added Ringer's solution and also, their $I_{corr}$ values were lower with respect to the Ringer's solution with 0.1M NaF. The specimens aged at 500, 600 and 800 $^{o}$C were seemed to form passive layer as shown in Figure 5.10(b) but their $I_{pas}$ and $E_{pas}$ values were higher than for all surface and medium conditions. When the corrosion rates were determined in Table 5.4, only

the specimen aged at 600 $^{o}$C exhibited higher corrosion resistance at equilibrium corrosion conditions which was supported by the graph during anodic polarization experiment in Figure 5.10(b). Huang [61] also mentioned the increase of $I_{corr}$, $I_{pas}$ and $E_{corr}$ in the anodic direction with the addition of NaF more than 0.1M and detected $Na_2TiF_6$ compound on the surface of the passive layer of Ti-6Al-4V alloy by X – Ray photoelectron spectrometer (XPS). The polarization resistance, $R_p$, values, which were given in Table 5.4, were higher due to the neutral corrosion environment, where Huang had a media with pH 5.

# CHAPTER 6

## CONCLUSION

The aim of this study was to investigate the electrochemical behavior of Ti-6Al-4V ELI alloy in simulated body fluid, Ringer's solution, according to the underlied microstructure obtained by different heat treatments. For this purpose, a heat treatment schedule was prepared and corrosion tests were performed with these specimens.

The microstructructural characterizations exhibited that according to the cooling rates from beta transus temperature, different microstructures formed which were equilibrium α (Widmanstätten α) and β phases for furnace cooling, basket–weave α for air cooling and α' martensite for water quenching. In addition, aging of martensite at different temperatures resulted that ~1wt% vanadium element removal from martensite phase and an increase in the width of martensite plates after 700 $^{o}$C. According to the vanadium element removal from martensite during aging procedure and replacement of vanadium with titanium atoms caused an expansion in the unit cell volume of the α phase. The lattice parameter "a" did not exhibit a characteristic behavior but "c" value increased continuously during aging at higher temperatures. However the variations in lattice parameters and unit cell volume did not point out a shift towards equilibrium α phase during aging. In addition, the minimum hardness values were obtained from Widmanstätten α phase in FC specimen.

The equilibrium corrosion characteristics of Ti-6Al-4V ELI alloy was investigated by measuring OCP in Ringer's solution at 37 $^{o}$C. The corrosion measurements exhibited that the passive film formation was seen for all

specimens where OCP values shifted to nobler values. Among all specimens, the nobler OCP value and the minimum corrosion rates belonged to FC specimen which indicated that the passive film formed on the surface of the FC specimen had more tendecy to prevent corrosion in equilibrium corrosion conditions. But in AC and WQ specimens, OCP values were active than FC specimen.

The passive film formation characteristics of the all heat treated specimens were investigated by anodic polarization method with as polished surface condition. During anodic polarization, WQ and WQ + Aged specimens were passivated at lower potentials and current densities than FC and AC specimens. The potentials were measured in a range of -203 mV to 2mV and the current densities were around $5x10^{-6}$ A/cm$^2$ for WQ and WQ + Aged specimens.

The stability of the previously formed passive film, which was formed under OCP conditions in Ringer's solution for four days, were studied by anodic polarization. The formation of the passive film was observed for all specimens. The passivation potential and corrosion density of FC specimen was measured nearly same as the as polished surface condition. The WQ and WQ + Aged specimens exhibited early passivations at lower passivation potentials and current densities to prevent dissolution of the film. Thus, a two step passivation at -240 mV and at -300 mV, and $(1.4 – 1.5)x10^{-6}$ A/cm$^2$, was seen. The previously formed passive film on AC specimen, however dissolved during anodic polarization. These indicated that the stability of the previously formed film on the WQ and WQ + Aged specimen were higher than the FC and AC specimens.

In addition, in order to understand the corrosion behavior of heat treated Ti-6Al-4V ELI alloy in the presence of $F^-$ ions, the NaF was added to the solution in the order of 0.1M and 0.2M, respectively. In the first case, the aggressive effect of $F^-$ ions was not observed clearly, but in the second case, the behavior of anodic oxide polarization was seen instead of an active to passive transition, especially for WQ specimen. According to the 0.2M NaF addition to the Ringer's solution

seemed to increase the corrosion rates by inhibiting passive film formation during anodic polarization.

# REFERENCES


[1] Leyens, C., Peters M., ed. "Titanium and Titanium Alloys - Fundamentals and Applications". WILEY - VCH Verlag GmbH & Co. KgaA: Weinheim, Germany, pp. 1 - 42, 454-455, 2003.

[2] Jones, D.A., "Principles and Prevention of Corrosion", Second ed. Upper Saddle River, NJ 07458, Prentice Hall, pp. 1-8, 40-48, 75-84, 146-156, 1996.

[3] Textor, M., Sittig, C., Frauchiger, V., Tosatti, S., Brunette, D. M., "Properties and Biological Significance of Natural Oxide Films on Titanium and Its Alloys", in Titanium in Medicine, M. D., Brunette, P., Tengvall, M., Textor, P., Thomsen, Editor, Springer - Verlag Berlin, pp. 171-230, 2001.

[4] Lütjering, G., Williams, J. C., Gysler, A., "Microstructure and Mechanical Properties of Titanium Alloys", in Microstructure and Properties of Materials, J.C.M. Li, Editor, World Scientific Publishing, pp. 1-25, 2000.

[5] Donachie, M.J., Jr., "Titanium - A Technical Guide". Metals Park, OH 44073, ASM International, pp. 2 - 6, 1988.

[6] Williams, J.C., "Titanium: Alloying", in Encyclopedia of Materials Science and Engineering, M.B. Bever, Editor, Pergamon Press, USA, pp. 5086-5089, 1986.

[7] ASM Committee, "Introduction to Titanium and Its Alloys", in ASM Metals Handbook, ASM International, Metals Park, Ohio, USA, pp. 351-417, 1980.

[8] Hammond, C., Nutting, J., "Physical Metallurgy of Superalloys and Titanium Alloys", Met. Technology, v4, pp. 474-490, 1977.

[9] Malinov, S., Sha, W., Guo, Z., Tang, C. C., Long, A. E., "Synchroton X-ray diffraction study of the phase transformations in titanium alloys", Materials Characterization, v48, pp. 279-295, 2002.

[10] Lütjering, G., "Influence of processing on microstructure and mechanical properties of (α + β) titanium alloys", Materials Science and Engineering A, v243, pp. 32-45, 1998.

[11] Gil, F.J., Ginebra, M. P., Manero, J. M., Planell, J. A., "Formation of α-Widmanstatten structure: effects of grain size and cooling rate on the Widmanstatten morphologies and on the mechanical properties in Ti-6Al-4V alloy", Journal of Alloys and Compounds, v329, pp. 142-152, 2001.

[12] Fujii, H., "Continuous Cooling Transformation Characteristics of α + β Titanium Alloys", Nippon Steel, no 62, pp. 74-79, 1994.

[13] Ahmed, T., Rack, H. J., "Phase transformations during cooling in α + β titanium alloys", Materials Science and Engineering A, v243, pp. 206-211, 1998.

[14] Lütjering, G., "Property optimization through microstructural control in titanium and aluminum alloys", Materials Science and Engineering A, v263, pp. 117-126, 1999.

[15] Tiley, J., Searles, T., Lee, E., Kar, S., Banerjee, R., Russ, J. C., Fraser, H. L., "Quantification of microstructural features in α / β titanium alloys", Materials Science and Engineering A, v372, pp. 191-198, 2004.

[16] Williams, J.C., Chesnutt J. C., "Titanium Alloys: Thermomechanical Treatment", in Encyclopedia of Materials Science and Engineering, M.B. Bever, Editor, Pergamon Press, USA, pp. 5094-5099, 1986.

[17] Ding, R., Guo, Z. X., Wilson, A., "Microstructural evolution of a Ti-6Al-4V alloy during thermomechanical processing", Materials Science and Engineering A, v327, pp. 233-245, 2002.

[18] Pederson, R., "Microstructure and Phase Transformation of Ti-6Al-4V", M.S. Thesis, Department of Applied Physics and Mechanical Engineering Division of Engineering Materials, Luleå University of Technology, Luleå, 2002.

[19] Zeng, L., Bieler T. R., "Effects of working, heat treatment, and aging on microstructural evolution and crystallographic texture of α, α', α" and β phases in Ti-6Al-4V wire", Materials Science and Engineering A, v392, pp. 403-414, 2005.

[20] Ivasishin, O.M., Teliovich, R. V., "Potential of rapid heat treatment of titanium alloys and steels", Materials Science and Engineering A, v263, pp. 142-154, 1999.

[21] Stanford, N., Bate, P. S., "Crystallographic variant selection in Ti-6Al-4V", Acta Materialia, v52, pp. 5215-5224, 2004.

[22] Semiatin, S.L., Fagin, P. N., Glavicic, M. G., Sukonnik, I. M., Ivasishin, O. M., "Influence on texture on beta grain growth during continuous annealing of Ti-6Al-4V", Materials Science and Engineering A, v299, pp. 225-234, 2001.

[23] Ivasishin, O.M., Shevchenko, S. V., Semiatin, S. L., "Effect of crystallographic texture on the isothermal beta grain-growth kinetics of Ti-6Al-4V", Materials Science and Engineering A, v332, pp. 343-350, 2002.

[24] Malinov, S., Markovsky, P., Sha, W., Guo, Z., "Resistivity study and computer modelling of the isothermal transformation kinetics of Ti-6Al-4V and Ti-6Al-2Sn-4Zr-2Mo-0.08Si alloys", Journal of Alloys and Compounds, v314, pp. 181-192, 2001.

[25] Jovanović, M.T., Tadić, S., Zec, S., Mišković, Z., Bobić, I., "The effect of annealing temperatures and cooling rates on microstructure and mechanical properties of investment cast Ti-6Al-4V alloy", Materials and Design v27, no 3, pp. 192-199, 2006.

[26] Gil, F.J., Planell, J. A., "Behaviour of normal grain growth kinetics in single phase titanium and titanium alloys", Materials Science and Engineering A, v283, pp. 17-24, 2000.

[27] Filip, R., Kubiak K., Ziaja W., Sieniawski J., "The effect of microstructure on the mechanical properties of two-phase titanium alloys", Journal of Materials Processing Technology, v133, pp. 84-89, 2003.

[28] Sha, W., Guo, Z., "Phase Evolution of Ti-6Al-4V during continuous heating", Journal of Alloys and Compounds, v290, pp. L3-L7, 1999.

[29] Borgioli, F., Galvanetto, E., Fossati, A., Pradelli, G., "Glow-Discharge and Furnace Treatments of Ti-6Al-4V", Surface and Coatings Technology, v184, pp. 255-262, 2004.

[30] Alvarado, C.D., "A Study of the Corrosion Resistance of Gama Titanium Aluminide in Ringer's Solution, 3.5 wt% NaCl and Seawater", M.S. Thesis, Mechanical Engineering, University of Puerto Rico Mayagüez Campus, Puerto Rico, pp. 1-7, 28-36, 47-82, 2005.

[31] Song, Y., Zhu, X., Wang, X., Che, J., Du, Y., "Anodic oxidation behaviour of Al-Ti alloys in acidic media", Journal of Applied Electrochemistry, v31, pp. 1273-1279, 2001.

[32] Nowak, S.B., Sun, E. X., "Electrochemical characteristics of Ti-6Al-4V alloy in 0.2 N NaCl solution. II. Kinetic behaviors and electric field in passive film", Corrosion Science, v43, pp. 1817-1838, 2001.

[33] Robin, A., Rosa, J. L., Sandim, H. R. Z., "Corrosion behaviour of Ti-4Al-4V alloy in nitric, phosphoric and sulfuric acid solutions at room temperature", Journal of Applied Electrochemistry, v31, pp. 455-460, 2001.

[34] Aziz-Kerrzo, M., Conroy Kenneth, G., Fenelon, A. M., Farrell, S. T., Breslin, C. B., "Electrochemical studies on the stability and corrosion resistance of titanium-based implant materials", Biomaterials, v22, pp. 1531-1539, 2001.

[35] Basame, S.B., White, H. S., "Pitting Corrosion of Titanium – The Relationship Between Pitting Potential and Competitive Anion Adsorption at the Oxide Film/Electrolyte Interface", Journal of The Electrochemical Society, v147, no 4, pp. 1376-1381, 2000.

[36] Codaro, E.N., Nakazato, R. Z., Horovistiz, A. L., Ribeiro, L. M. F., Ribeiro, R. B., Hein, L. R. O., "An image analysis study of pit formation on Ti-6Al-4V", Materials Science and Engineering A, v341, pp. 202-210, 2003.

[37] Morris, P.E., "Measurement of Pit Initiation and Propagation for Iron-Chromium-Nickel Alloys in Acid Chloride Environments by Electrochemical Techniques", in Electrochemical Techniques for Corrosion Engineering, R. Baboian, Editor, NACE, Houston, Texas, pp. 287-295, 1986.

[38] Mudali, U.K., Sridhar, T. M., Raj, B., "Corrosion of bio implants", Sādhanā, v28, no 3&4, pp. 601-637, June/August 2003.

[39] Gurappa, I., "Characterization of different materials for corrosion resistance under simulated body fluid conditions", Materials Characterization, v49, pp. 73-79, 2002.

[40] Cai, Z., Nakajima, H., Woldu, M., Berglund, A., Bergman, M., Okabe, T., "In vitro corrosion resistance of titanium made using different fabrication methods", Biomaterials, v20, pp. 183-190, 1999.

[41] Cai, Z., Shafer, T., Watanabe, I., Nunn, M. E., Okabe, T., "Electrochemical characterization of cast titanium alloys", Biomaterials, v24, pp. 213-218, 2003.

[42] Kuphasuk, C., Oshida, Y., Andres, C. J., Hovijitra, S. T., Barco, M. T., Brown, D. T., "Electrochemical corrosion of titanium and titanium-based alloys", Journal of Prosthetic Dentistry, v85, pp. 195-202, 2001.

[43] Ibriş, N., Rosca, J. C. M., "EIS study of Ti and its alloys in biological media", Journal of Electroanalytical Chemistry, v526, pp. 53-62, 2002.

[44] Choubey, A., Basu, B., Balasubramaniam, R., "Electrochemical Behaviour of Ti-Based Alloys in Simulated Human Body Fluid Environment", Trends Biomaterials:Artif. Organs, v18, no 2, pp. 64-72, 2005.

[45] López, M.F., Gutiérrez, A., Jiménez, J. A., "In vitro behaviour of titanium alloys without vanadium", Electrochimica Acta, v47, pp. 1359-1364, 2002.

[46] Metikoš-Huković, M., Kwokal, A., Piljac, J., "The influence of niobium and vanadium on passivity of titanium-based implants in physiological solution", Biomaterials, v24, pp. 3765-3775, 2003.

[47] Mareci, D., Bocanu, C., Nemtoi, G., Aelenei, D., "Electrochemical behaviour of titanium alloys in artificial saliva", J. Serb. Chem. Soc., v70, no 6, pp. 891-897, 2005.

[48] Al-Mayaouf, A.M., Al-Swayih, A. A., Al-Mobarak, N. A., Al-Jabab, A. S., "The effect of fluoride on the electrochemical behavior of Ti and some of its alloys for dental applications", Materials and Corrosion, v55, no 7, pp. 524-530, 2004.

[49] Burstein, G.T., Liu, C., Souto, R. M., "The effect of temperature on the nucleation of corrosion pits on titanium in Ringer's physiological solution", Biomaterials, v26, pp. 245-256, 2005.

[50] Sittig, C., Marti, A. H., Textor, M., Spencer, N. D., "The implant material, Ti-6Al-7Nb: surface microstructure, composition and properties", Journal of Materials Science: Materials in Medicine, v10, pp. 191-198, 1999.

[51] Geetha, M., Mudali, U. K., Gogia, A. K., Asokamani, R., Raj, B., "Influence of microstructure and alloying elements on corrosion behaviour of Ti-13Nb-13Zr alloy", Corrosion Science, v46, no 4, pp. 877-892, 2004.

[52] Bearinger, J.P., Orme, C. A., Gilbert, J. L, "In situ imaging and impedance measurements of titanium surfaces using AFM and SPIS", Biomaterials, v24, pp. 1837-1852, 2003.

[53] Stern, M., Geary, A. L., "Electrochemical Polarization", Journal of the Electrochemical Society, v104, no 1, pp. 56, 1957.

[54] Dynamic Machine Work Inc., "Titanium 6Al-4V Tubular Products"; http://www.flowform.com/metallurgical_and_mechanical_p.html, May 2006.

[55] Mansfeld, F., "Simultaneous Determination of Corrosion Rates and Tafel Slopes from Polarization Resistance Measurements", Journal of Electrochemical Society, v120, pp. 515, 1973.

[56] Schmitz-Pranghe, N., Dünner, P., "Gitterstruktur und thermische Ausdehnung der Übergangsmetalle Scandium, Titan, Vanadin und Mangan", Zeitschrift fuer Metallkunde, v59, pp. 377-382, 1968.

[57] Elmer, J.W., Palmer, T. A., Babu, S. S., Specht E. D., "In situ observations of lattice expansion and transformation rates of α and β phases in Ti-6Al-4V", Materials Science and Engineering A, v391, pp. 104-113, 2005.

[58] Milosev, I., Metikos-Hukovic, M., Strehlblow, H. H., "Passive film on orthopedic TiAlV alloy formed in physiological solution by X - Ray photoelectron spectroscopy", Biomaterials, v21, no 20, pp. 2103-2113, 2000.

[59] Ask, M., Lausmaa, J., Kasemo, B., "Preparation and surface spectroscopic characterization of oxide films on Ti-6Al-4V", Applied Surface Science, v35, no 3, pp. 283-301, 1989.

[60] Schmidt, A.M., Azambuja, D. S., "Effect of Fluoride Ions on Ti-6Al-4V Alloy Passivation in Lactated Ringer's Serum", Materials Research, v6, no 2, pp. 227-231, 2003.

[61] Huang, H.H., "Effect of fluoride and albumin concentration on the corrosion behavior of Ti-6Al-4V alloy", Biomaterials, v24, no 2, pp. 275-282, 2003.